Title
FOURIER TRANSFORM NUCLEAR QUADRUPOLE RESONANCE SPECTROSCOPY

Authors
Klainer, S.M.
Hirschfeld, T.B.
Marino, R.A.

Publication Date
1981-11-01

Lawrence Berkeley Laboratory
UNIVERSITY OF CALIFORNIA

EARTH SCIENCES DIVISION

To be published as a Book Chapter in Fourier, Hadamard and Hilbert Transforms in Chemistry, Plenum Press, December 1981

FOURIER TRANSFORM NUCLEAR QUADRUPOLE RESONANCE SPECTROSCOPY

Stanley M. Klainer, Tomas B. Hirschfeld, and Robert A. Marino

November 1981

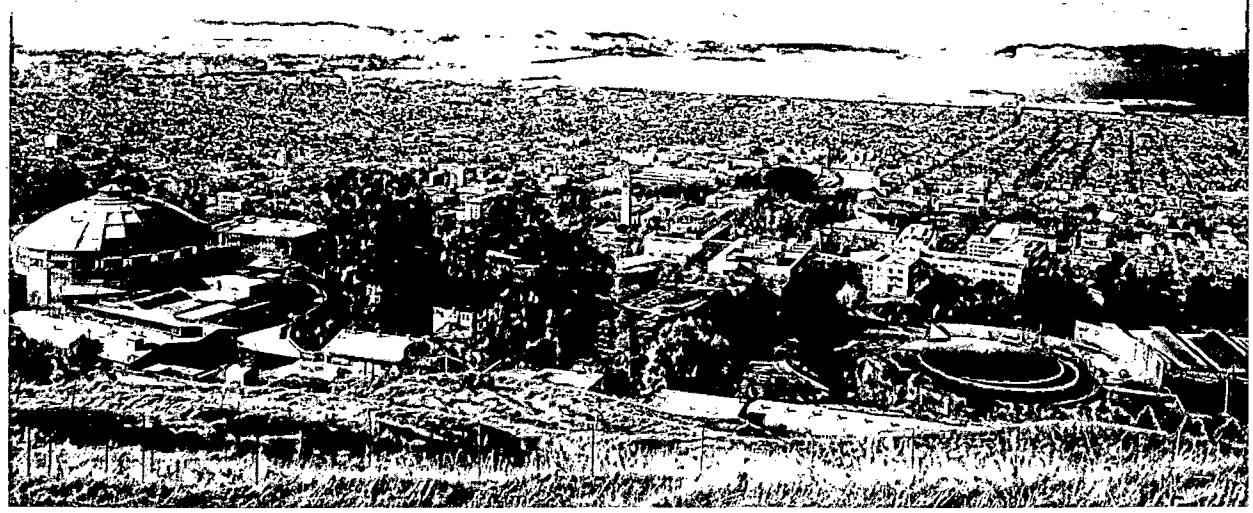

Prepared for the U.S. Department of Energy under Contract W-7405-ENG-48

DISCLAIMER

LBL-13570

FOURIER TRANSFORM NUCLEAR QUADRUPOLE RESONANCE SPECTROSCOPY

Stanley M. Klainer**, Tomas B. Hirschfeld+, and Robert A. Marino++

Earth Sciences Division
Lawrence Berkeley Laboratory
University of California
Berkeley, CA 94720

November 1981

This work was supported in part by the U.S. Department of Energy under Contract No. W-7405-ENG-48 and the U.S. Army Research Office under Contract No. DAAG-29-79-0025.

ABSTRACT

Pulsed NQR (Nuclear Quadrupole Resonance) spectroscopy is the most recent technique to use the signal-to-noise advantage of the FT (Fourier Transform) data handling and processing method. The combination of pulsed and FT methods has made it possible for NQR to be routinely applied to analytical tasks.

The advantages of FT-NQR will be discussed. State-of-the-art FT-NQR systems will be described and specific areas of current instrument research will be detailed. Several practical applications of FT-NQR to Nitrogen-14 containing compounds will be presented. Other potential applications of NQR, using various probe nuclei, will be addressed and compared to other analytical methods.

FOURIER TRANSFORM NUCLEAR QUADRUPOLE RESONANCE SPECTROSCOPY

by

Stanley M. Klainer,** Tomas B. Hirschfeld+
and Robert A. Marino++

I. INTRODUCTION

FT-NQR (Fourier Transform Nuclear Quadrupole Resonance) spectroscopy is one of the newer analytical tools. Although nuclear quadrupole coupling constants were first observed in atoms by Schmidt and Schuler[1] in 1935 and in molecules by Kellog[2] and coworkers in 1936, it was the discovery of pure quadrupole coupling transitions in solids by Dehmelt and Kruger[3][4] in 1950 and 1951 that initiated the understanding of the NQR phenomenon as presently utilized.

During the past 30 years the growth of NQR has been anything but phenomenal. A great quantity of theoretical work has been reported but the experimental investigations have been restricted primarily to nitrogen-containing and halogenated compounds. How, then, can an application paper, such as this be justified? The answer lies in responding to two specific questions:

(a) What has hindered the growth of NQR to date and can this be overcome with present day technology?

---

*Tnis work was supported in part by the U. S. Department of Energy under Contract No. W-7405-ENG-48 and U. S. Army Research Office under Contract No. DAAG-29-79-0025.

**Lawrence Berkeley Laboratory, 90/1140, Berkeley, CA 94720.

+Lawrence Livermore National Laboratory, L325, Livermore, CA 94550.

++Hunter College of CUNY, 695 Park Avenue, New York, N.Y. 10021.

(1) H. Schuler and T. Schmidt, Z. Phys. 94, 457 (1935).

(2) J. M. B. Kellog, I. I. Rabi, N. F. Ramsey and J. R. Zacharias, Phys. Rev. 55, 728 (1936).

(3) H. G. Dehmelt and H. Kruger, Naturwiss. 37, 111 (1950).

(4) H. G. Dehmelt and H. Kruger, Naturwiss. 38, 921 (1951).

(b) Why is it important that NQR be developed as a practical analytical technique at this time?

In responding to these queries, it is possible to show that FT-NQR is both needed and implementable.

This paper is directed at the applied scientist, and, therefore, it does not contain the in-depth theoretical and mathematical information of interest to the research scientist. Texts by Schempp and Bray[5], Lucken[6], Slichter[7] and Biryukov, Voronkov and Safin[8] can supplement the information on NQR presented in this paper. There is, however, no primer on FT-NQR and the basic concepts of this specific area will be addressed in this discussion.

II. NQR SPECTROSCOPY

Nuclear Quadrupole Resonance (NQR) is a branch of radio-frequency spectroscopy. The NQR spectrometer detects the interaction of a nuclear quadrupole moment with the electric field gradient (EFG) produced by the charge distribution in a solid state compound. The quadrupole moment arises because the nuclear charge distribution is nonspherical. Resonance occurs when transitions from one spin state to another are excited by radio-frequency electro-magnetic oscillations. In this way, NQR is quite similar in principle to nuclear

---

[5] E. Schempp and P. J. Bray, "Nuclear Quadrupole Resonance Spectroscopy", Physical Chemistry, an Advanced Treatise, Volume 4, Academic Press, New York (1970).

[6] E. A. C. Lucken, "Nuclear Quadrupole Coupling Constants", Academic Press, New York (1969).

[7] C. P. Slichter, "Principles of Magnetic Resonance", Second Edition, Springer Series in Solid-State Sciences 1, Springer-Verlag, Berlin, Heidelberg, New York (1978).

[8] I. P. Biryukov, M. G. Voronkov and I. A. Safin, "Tables of Nuclear Quadrupole Resonance Frequencies", Israel Program for Scientific Translations, Jerusalem (1969).

magnetic resonance (NMR). In NQR, however, the energy levels depend on the coupling of the nuclear moment to the internal electric field gradient, whereas in NMR they are primarily dependent on the coupling of the nuclear magnetic moment with an external magnetic field. Since the EFG is a very sensitive function of the molecular and crystal structure, the resonance frequencies and band shapes are specific to each compound, and NQR data can be used for determining unambiguous sample identification, local electronic structure, atomic arrangement, order/disorder phenomena, and crystal phase transformations. In addition, molecular dynamics in the solid state can be studied. Furthermore, since NQR data are sensitive to changes in temperature and pressure, there is the possibility of obtaining strain information.

A. Basic Concept of NQR

In order to understand the origin of nuclear quadrupole resonance, it is usual to visualize the nucleus as a classical distribution of positive charges, $\rho_N(\vec{r})$, over a volume of characteristic dimensions on the order of nuclear radii, i.e. 10^{-13} cm (Figure 1). On the other hand, a charge cloud extending over a volume on the order of several angstroms (10^{-8}cm) generates an electrostatic potential $\phi(\vec{r})$ which can be considered as varying slowly over the region occupied by the nucleus. The electrostatic energy W of the system can be expressed (7) as:

$$W = \int \rho_N(\vec{r})\phi(\vec{r})d\vec{r} \ , \tag{1}$$

which can be expanded in terms of the moments of the nuclear charge distribution:

$$W = -\phi(0)q_N + \vec{p}\cdot\vec{E}(0) - \frac{1}{6}\sum_{ij} q_{ij}Q_{ij} + \cdots \tag{2}$$

where (o) means evaluated at the origin, the center of mass of the nucleus, and

$$q_N = \int \rho_N(\vec{r})\,d\vec{r} \qquad \text{nuclear charge}$$

$$\vec{p} = \int \rho_N(\vec{r})\,\vec{r}\,d\vec{r} \qquad \text{nuclear dipole moment vector}$$

$$Q_{ij} = \int \rho_N(\vec{r})\,x_i x_j\,d\vec{r} \qquad \text{nuclear quadrupole moment tensor}$$

$$\vec{E} = -\vec{\nabla}\phi \qquad \text{external electric field vector}$$

$$q_{ij} = (\partial E_i/\partial x_j)_o \qquad \text{external electric field gradient tensor}$$

From quantum mechanical considerations it can be proven that the only non-vanishing terms in Eqn. 2 are the first, third, and other odd-ordered ones. The first term is simply a constant, and, therefore, the orientationally-dependent term in the energy is the quadrupolar energy (hexadecapole interactions are extremely small if they exist at all):

$$W_Q = \frac{1}{6} \sum_{ij} q_{ij} Q_{ij} \tag{3}$$

Q_{ij} is diagonal and is related to the components of the nuclear spin I_i according to:

$$Q_{ii} = \frac{eQ}{I(2I-1)} \left[3I_i^2 - I(I+1) \right] \tag{4}$$

where $I = \left(\sum I_i^2\right)^{1/2}$ is the nuclear spin and $\underline{eQ}$ is defined as the nuclear quadrupole moment. Since $\nabla^2\phi = 0$ by the Laplace equation, we have

$$\sum_i q_{ii} = 0 .$$

The quantum mechanical expression for the quadrupole energy (the Hamiltonian) takes the particularly simple form:

$$H_Q = \frac{eQ}{2I(2I-1)} \sum_i q_{ii} I_i^2 , \tag{5}$$

which can also be expressed in the form:

$$H_Q = \frac{e^2qQ}{4I(2I-1)} \left[\left(3I_z^2 - I^2 \right) + \eta \left(I_x^2 - I_y^2 \right) \right] \qquad (6)$$

where I and I_j are spin operators.

The quantity e^2qQ is called the quadrupole coupling constant of the system and η is defined as the asymmetry parameter of the electric field gradient (EFG):

$$\eta \equiv \frac{q_{xx} - q_{yy}}{q_{zz}} \quad , \text{ and}$$

$$eq \equiv eq_{zz} \quad \text{so} \quad e^2qQ = (eQ)(eq_{zz}) \qquad (7)$$

when the axes are labelled

$$|q_{zz}| \geq |q_{yy}| \geq |q_{xx}| \qquad \text{by convention.}$$

For nitrogen-14, with nuclear spin I = 1, the solution of the Schroedinger equation $H_Q \Psi_N = E_N \Psi_N$, where Ψ_N is the nuclear wave function, can be shown to lead to a three level system of energies given by

$$E_z = e^2qQ/2$$
$$E_x = -E_z(1-\eta)/2$$
$$E_y = -E_z(1+\eta)/2 \qquad (8)$$

Transitions between these levels can be induced with oscillating magnetic fields of the proper (resonant) frequencies (Figure 2). The frequencies of these transitions are

$$\nu_+ = \frac{e^2qQ}{4h}(3+\eta)$$
$$\nu_- = \frac{e^2qQ}{4h}(3-\eta)$$
$$\nu_d = \frac{e^2qQ\eta}{2h} = \nu_+ - \nu_- \qquad (9)$$

Determining any two of the three NQR frequencies completely describes the magnitude of the EFG in the vicinity of the nitrogen nucleus:

$$e^2qQ = \frac{2}{3}(\nu_+ + \nu_-)$$

$$\eta = \frac{2(\nu_+ - \nu_-)}{e^2qQ} \tag{10}$$

As another example, for nuclei of spin I = 5/2, such as aluminum-27, the solution of the Schroedinger equation can be shown to lead to a three-level system of energies[6] given by solutions of the secular equation[9]

$$E^3 - 7(3 + \eta^2)E - 20(1 - \eta^2) = 0, \tag{11}$$

where E is in units of $e^2qQ/20$. For the case, $\eta = 0$, the energies of the three eigenstates are:

$$E\left(\pm \frac{1}{2}\right) = -4\,\frac{e^2qQ}{20}$$

$$E\left(\pm \frac{3}{2}\right) = -1\,\frac{e^2qQ}{20}$$

$$E\left(\pm \frac{5}{2}\right) = +5\,\frac{e^2qQ}{20}\ . \tag{12}$$

The frequencies of the resultant allowed transitions are given by:

$$\nu_1 = \nu\left(\frac{3}{2} \to \frac{1}{2}\right) = \frac{3}{20}\,\frac{e^2qQ}{h}$$

$$\nu_2 = \nu\left(\frac{5}{2} \to \frac{3}{2}\right) = \frac{6}{2}\,\frac{e^2qQ}{h} \tag{13}$$

For the general case, $\eta \neq 0$, no solution in closed form can be written down. However, tables of the results of numerical solution of the eigenvalue

---

(9)T. P. Das and E. L. Hahn, "Nuclear Quadrupole Resonance Spectroscopy," Solid State Physics, Supplement 1, Academic Press, New York (1958). (Note that the error in the secular equation for spin 5/2 given on page 13 has been corrected.)

problem for $0 \leq \eta \leq 1$ in steps of .001 are available[10], so that observation of two NQR frequencies uniquely determines both the quadrupole coupling constant, e^2qQ, and the asymmetry parameter, η, of the site under study. For large values of η, it becomes theoretically possible to observe the "forbidden" transition corresponding to the sum of ν_1 and ν_2 in Equation 10. This may be especially useful to do in situations of low quadrupole coupling.

As an additional example, for nuclei of spin I = 7/2, such as uranium-235, the solution of the Schroedinger equation can be shown to lead to a five-level system of energies given by solutions of the secular equation[5],

$$E^4 - 42\,(1 + \eta^2/3)\,E^2 - 64\,(1 - \eta^2)\,E + 105\,(1 + \eta^2/3)^2 = 0$$

where E is in units of $e^2qQ/28$.

For the general case, $\eta \neq 0$ no solution in closed form can be written. However, tables of the results of numerical solution of the eigenvalue problem for $0 \leq \eta \leq 1$ in steps of .001 are also available[10], so that observation of two identified NQR frequencies again uniquely determines both the quadrupole coupling constant, e^2qQ, and the asymmetry parameter, η, of the site under study.

B. Experimental Techniques

Experimental techniques for the determination of NQR spectra can be divided into three categories:

a. Continuous-wave (CW) methods,

b. Transient methods, and

c. Double resonance techniques.

CW methods have enjoyed great popularity for they are simple and inexpensive. The limitations of these techniques are so severe, however,

---

[10] R. Livington and H. Zeldes, "Tables of Eigenvalues for Pure Quadrupole Spectra, Spin 5/2 and 7/2," Oak Ridge National Laboratory Report ORNL-1913 (1955).

that in the low MHz region they are rarely used anymore. Transient methods include the superregenerative technique (unproductive at the low frequencies of interest in many applied problems) and pulsed methods. Double resonance techniques are essentially pulsed methods that monitor the resonance of one type of nuclear species while another is being perturbed.[7] When applicable, these methods are extremely sensitive and are very convenient for locating unknown resonances, although lineshapes are not always reliable. Interested readers are referred to the excellent review by Edmonds.[11]

Pulsed techniques that operate in the so-called spin-echo mode are particularly good for applied NQR and they naturally lend themselves to remote detection.[12]

To understand the reasons for the advantage of the pulsed method (13-17) it is necessary to begin by defining some basic magnitudes that describe an NQR line. In the frequency domain an NQR line is fully described by its frequency and by a normalized shape function $S(\omega)$. For example:

$$S(\omega) = \frac{2}{\pi\Delta\omega} \frac{1}{1 + \left(\frac{\omega - \omega_o}{\Delta\omega}\right)^2} \qquad (14)$$

---

[11] D. T. Edmonds, Physics Reports 29, 233 (1977).

[12] T. Hirschfeld and S. M. Klainer, J. Mol. Struc. 58, 63 (1980).

[13] A. Zussman and S. Alexander, J. Chem. Phys. 49, 3792 (1968).

[14] G. Petersen and T. Oja, "Advances in Nuclear Quadrupole Resonance", (J. A. S. Smith, Ed.) 1, 179, Heyden, London (1974)

[15] Y. Abe, Y. Ohneda, M. Hirota and S. Kojima, J. Phys. Soc. Japan 37, 1061 (1974).

[16] A. Colligiani and R. Ambrosetti, Gazz. Chim. It. 106, 439 (1976).

[17] A. A. V. Gibson, R. Goc and T. A. Scott., J. Mag. Res. 24, 103 (1976).

However, spin-echo techniques operate in the time domain; here there are three parameters that describe an NQR absorption line:

a. Spin-lattice relaxation time, T_1. The characteristic time with which a bulk magnetization is established and energy can flow between the spin system and the lattice.

b. Spin-spin relaxation time, T_2. The characteristic time which describes the coupling between nuclei and which establishes the time scale for the observation of spin echoes.

c. A spin-echo shape function, G(t). The "width" of this function is defined as $2T_2^*$. G(t) is the Fourier transform of the line-shape function, S(ω); thus $T_2^* \propto \frac{1}{\Delta\omega}$.

Continuous-wave (CW) and superregenerative methods are poor techniques for lines with large T_1 and/or large $\Delta\omega$ values (short T_2) associated with the NQR line (to avoid saturation in CW, the input power level has to be reduced to very small values). Broad lines, expected to be important in applied NQR, are weak since their areas are constant. Spin-echo wide-line methods are not only unaffected by long T_1 values, but since G(t) and S(ω) are related by a Fourier transformation, the equality

$$G_{MAX} = \int_0^\infty S(\omega)\, d\omega = 1 \qquad (15)$$

holds (Fig. 3). Thus, broad lines in the frequency domain do not affect the maximum intensity of the echo signal.

The NQR spectrum of a substance is determined by placing about 25 grams of sample inside the inductor of a tank circuit, which is then subjected to a series of radio-frequency pulses of frequency f. Whenever the frequency of of these pulses satisfies the resonance condition $f = \nu_Q$, where ν_Q is one

of the quadrupole frequencies, absorption of energy takes place and is re-transmitted as a series of signals [free induction decay (FID) or spin echo]. Therefore, by monitoring and detecting the transmitted signals as a function of the frequency of the pulses, the energy levels of the quadrupole nucleus are completely determined. A number of different pulse sequences are possible; this results in more or less efficient signal production, depending on the values of the relaxation times.

III. NQR INSTRUMENTATION AND DATA HANDLING

For applied NQR spectroscopy pulsed techniques are used in conjunction with a variety of pulse sequences and FT data processing. This approach provides for maximum sensitivity and versatility.

A. Pulsed NQR Spectrometer

The most advanced pulsed NQR spectrometer in the nitrogen frequency region presently in operation was described by Harding et al.[18] in 1979. A block diagram of this instrument is shown in Fig. 4. This is an FT-NQR spectrometer which operates from 0.5 to 5MHz. The features of this instrument are:

(a) The use of heterodyne techniques throughout to eliminate carrier feed through.

(b) A matching network design that allows one-knob tuning of both the transmitter and receiver.

(c) The choice of several excitation sequences (Carr-Purcell, Meiboom-Gill modified Carr-Purcell, spin-locked spin-echo and the standard sequence of $\pi/2$ pulses) for generation and collection of signals at high data rates.

(d) Fast Fourier transform routines for studying line shapes, for

---

[18] J. C. Harding, D. A. Wade, R. A. Marino, E. G. Sauer and S. M. Klainer, J. Mag. Res. 36, 21 (1979).

facilitating spectral searches, and for improved sensitivity.

(e) Ability to handle small samples (0.1cc).[19]

The specifications for this instrument are given in Table I, column 1. This instrument, although state-of-the-art and much more versatile and sensitive than previous spectrometers, is not optimally suited to many applied NQR uses. A new system suited for practical NQR use is presently under design and scheduled for construction in early 1981. It's anticipated specifications are shown in Table I, column 2. When this instrument is operational, many of the obstacles which hinder NQR growth should be overcome.

B. Pulse Sequences

In order to optimize the NQR data format, it is necessary to choose the pulse sequence most suited for the measurement. Several of these exist and each has its benefits.

1) Free Induction Decay

The NQR response of a single crystal to a resonant pulse of rf irradiation is completely analogous to the spin 1/2 NMR case. One difference is that the intensity of the free induction decay (FID) response depends on the orientation of the radio-frequency field H_1 with respect to the EFG principal axes system. For a spin I = 1 system, the three resonance lines ν_+, ν_- and ν_d can be observed only when the field H_1 is oriented, respectively, along the x,y, and z principal axes of the EFG tensor. As an example, for a ν_- line, the expected value of the magnetization along the y axis is proportional to:

$$\frac{h\nu_-}{3kT} \sin(\sqrt{2}\omega_1 t_w) \cos(2\pi\nu_- t), \tag{16}$$

---

[19] R. A. Marino, J. C. Harding and S. M. Klainer, J. Mol. Struc. 58, 79 (1980).

Table I

PULSED FT-NQR SPECTROMETER

Specification	Existing System[a]	System Under Design
Frequency Range	0.5 to 5MHz	0.5 to 64 MHz
Sample Volume	40 to 0.1cc[b]	100 to 5×10^{-4}cc
System Sensitivity(SLSE)[c] S/N = 3, 1 sec integration	200 mg	1 mg
System Recovery Time (Sample Q=120)	150 µsec @ 3MHz	<15 µsec @ 1MHz
$\pi/2$ Pulse Width	50 µsec	10 µsec
Sample Coils	1 per octave	Same
Matching Networks	1 per octave	Same
Sample Operating Temperature	77°K to 350°K	4°K to 350°K
Remote Detection	Yes, non-directional	Yes, directional
Automatic Spectral Search	No	Yes, programmed sequence

a) Reference (18)

b) Reference (19)

c) Reference (21)

where $\omega_1 = \gamma H_1$ measures the intensity of the irradiation, and t_w is the duration of the irradiating pulse. The maximum response is obtained when:

$$\sqrt{2}\omega_1 t_w = \sqrt{2}\gamma H_1 t_w = \pi/2 \qquad (17)$$

in analogy with the NMR case.

In NQR, however, the sample usually consists of a polycrystalline powder. Then a convolution for all orientations must be made. The result[20] is that the $\sin(\sqrt{2}\omega_1 t_w)$ function in the expression for the expectation value of the magnetization becomes a Bessel function, $J_1(\sqrt{2}\omega_1 t_w)$. This function has its first maximum, analogous to a "90° pulse" at $\sqrt{2}\omega_1 t_w = 0.66\pi$ and not at $0.5\ \pi$ like the sine function. Similarly, the first null, corresponding to a "180° pulse" occurs for a value of the argument equal to 1.43π rather than simply to π.[20]

2) Spin Echo and Carr-Purcell (CP) Sequence

Following a FID experiment in a case where T_2 (spin-spin relaxation time) $>T_2^*$ (spin echo shape function) it is possible to recall part of the magnetization not lost through T_2 processes by applying a "180° pulse" at a time τ after the first pulse. As is well known, an echo will form at a time 2τ and this echo can be repeatedly recalled at integral multiples of this time $2n\tau$ by the application of additional "180° pulses" at times $(2n-1)\tau$. The amplitude of the resultant echo train decays with time constant T_2 (Fig. 5). Signal-to-noise enhancement can be obtained by coherently adding successive echoes in the sequence. The optimum time for co-addition is easily shown to be $1.26T_2$. Due to the generally small value of T_2 in solids, however, this method does not result in an appreciable enhancement of the signal-to-noise ratio.

---

[20] G. L. Petersen, Ph.D. Thesis, Brown University (1975).

3) Spin-Lock Spin-Echo (SLSE)

A major advance in S/N enhancement was made by Marino and Klainer[21] when an adaptation of the Ostroff-Waugh sequence[22] was made to NQR. The sequence needed is essentially a Meibrom-Gill-modified-CP sequence where all the pulses have the same flip angle of "90°", which means 0.66π in the NQR of an I = 1 nucleus. In Fig. 6 ($NaNO_2$ at 77°K, on resonance) and Fig. 7 ($NaNO_2$ at 77°K, slightly off resonance) it can be seen that the spin echo train in this sequence persists for times of order T_1 (spin lattice relaxation time, actually $T_{1\rho}$) and not the much shorter T_2. Coherent addition of the echoes in this case results in considerable enhancement of the S/N, since $T_{1\rho} >> T_2$ is the typical situation in these solids. Marino and Klainer showed that the optimum enhancement is $0.64\ (T_{2\varepsilon}/2\tau)^{1/2}$ where $T_{2\varepsilon}$ is the effective decay constant of the echo train and 2τ is the spacing between echoes, or equivalently the spacing between pulses of the excitation sequence. It was further shown that the NQR effect was completely analogous to the spin 1/2 NMR case discussed by Waugh[23] in that the decay constant $T_{2\varepsilon}$ tends to $T_{1\rho}$ as τ is reduced to values less than T_2. Furthermore, for intermediate values of $T_{2\varepsilon}$, this parameter is proportional to τ^{-5}, again in analogy to NMR. Fig. 8 shows this functional dependence for $NaNO_2$ at 77°K. Recently, Cantor and Waugh[24] have developed a theory to explain the main features of this NQR effect using a model of a polycrystalline solid with each nitrogen site having one nearest neighbour.

---

(21) R. A. Marino and S. M. Klainer, J. Chem. Phys. 67, 3388 (1977).

(22) E. D. Ostroff and J. S. Waugh, Phys. Rev. Letters, 16, 1097 (1966).

(23) J. S. Waugh, J. Mol. Spec. 35, 298 (1970).

(24) R. S. Cantor and J. S. Waugh, J. Chem. Phys. 73, 1054 (1980).

4) Strong Off-Resonance Comb (SORC)

Recently a new pulsed NQR experiment has been used by one of the authors (RAM) which can have considerable advantages in enhancing the S/N ratio of weak lines. This represents new and yet unpublished information.

The steady state response of an ensemble of nuclear spins, I = 1/2, in high magnetic field H_o to a strong radio-frequency field H_1, applied off resonance by Δf, has long been known[7]. When all the conditions for the establishment of a spin temperature in the rotating frame are met[7], the x-component of the magnetization, which is experimentally observable, is given by the expression:

$$M_x = M_o \left[\frac{H_1 (2\pi\Delta f/\gamma)}{H_1^2 + H_{loc}^2 + (2\pi\ \Delta f/\gamma)^2} \right] \qquad (18)$$

where M_o is the equilibrium longitudinal magnetization, γ is the magnetogyric ratio of the nucleus, and H_{loc} is a measure of the local field at the nuclear site due to its neighbors. Results analogous to Eqn. 18 have also been derived and observed for a quadrupolar system[25] with nuclear spin I = 3/2 when subjected to the same strong, long, off-resonant irradiation H_1.

The preliminary results obtained, when the irradiation field H_1 is applied in a long train of equally-spaced identical pulses, are presented here. Although the SORC experimental data reported here are for a quadrupolar I = 1 system, analogous effects in a magnetic system or a quadrupolar system with spin different from unity can be expected.

Fig. 9a defines the parameters of the SORC sequence. Here a train of radio-frequency pulses of duration t_w and spacing τ is applied, Δf

---

[25] J. C. Pratt, P. Raghunathan and C. A. McDowell, J. Chem. Phys. 61, 1016 (1974) and J. Mag. Res. 20, 313 (1975).

away from exact resonance, to a pure nuclear electric quadrupole system in zero external magnetic field.

The variation of the signal amplitude vs. Δf, the distance from exact resonance, shows two features as depicted in Figs. 9b and 9c. First, the signal amplitude is modulated by a sinusoid of period $1/\tau$, the pulse repetition rate. This phenomenon is best understood by considering that the Fourier transform of the transmitter pulses has periodicity $1/\tau$. This leads to successive maxima and minima in the NQR signal (Figs. 9b and c) as the transmitter frequency is changed, i.e., Δf is varied. Alternatively, and more naively, this modulation can be interpreted as the destructive interference of type I signals (immediately following the rf pulse) and type II signals (immediately preceeding the rf pulse) in their overlap region as the frequency, Δf, is slowly varied.

Another feature shown in Fig. 9c is the shape of the envelope, possibly conforming to a function of the type $\Delta f/(A^2 + \Delta f^2)$, such as Eqn. 18. Insufficient data have been taken so far to ascertain the degree of agreement with theory on this last point.

The nuclear induction signals present in the observation window between successive pulses of the SORC sequence are shown in Figs. 10a-j as a function of the pulse separation τ. All data were taken on the ν_- line of $NaNO_2$ at 77°K. The magnitude of the type I signal is then plotted vs. τ in Figure 11. Note that for $\tau \geqslant 8$ msec the magnitude of type I signals increases with τ as might be expected for a FID signal subject to spin-lattice relaxation. On the other hand, for $\tau \leqslant 5$ msec, signals at both ends of the observation window are of a comparable size and they grow exponentially with decreasing τ. This is the region of interest.

Fig. 12 shows the variation of the type II signal vs. $\langle H_1 \rangle$ for τ = 3 msec. The experimental points are obtained for four different values of the instantaneous field H_1 obtained by changing the pulse width t_w at constant "flip angle" $\sqrt{2}\ \gamma\ t_w H_1$. The dotted line is the curve $F = \langle H_1 \rangle / [\langle H_1 \rangle^2 + B^2]$ with B = 0.05 G. The fact that $\langle H_1 \rangle$, the average value, rather than H_1, the peak value, is the important parameter and that there is good agreement of the data with the form of Eqn. 18 is strong evidence that the ensemble of spins is responding to the time-average field of the SORC sequence in a manner analogous to the conventional long, strong, off-resonant pulse.

The size of the parameter B is found to be about 0.05G which is approximately two orders of magnitude too small for the value expected from the contribution of Δf to Eqn. 18. This discrepancy is reduced by a factor of 5 when the experiment is repeated for τ = 1 msec, as shown in Fig. 13. Comparison of Figs. 12 and 13 suggest that the pulse nature of the experiment is still very important for τ = 1 msec and that quantitative agreement cannot be expected until τ is reduced further.

The potential of this technique appears to be great since signals can be obtained at essentially 100% duty cycle. However, further experimentation is needed to completely understand the operational parameters of SORC.

C. FT Considerations

There are three main reasons for doing FT spectroscopy:

a. Enchancement of signal-to-noise over CW methods is given by the square root of the ratio of the total width of the spectrum to the typical line width, $\sqrt{T_2^* \Delta}$.

b. Pulsed methods are singularly well-suited to data processing.

c. The line shape is readily obtained directly from the output.

Of these, the first reason, probably the most important in other disciplines, is not nearly as important in NQR, because the ratio defined above is not large and can often be close to unity. This is so because in solids line widths are relatively large (a few kHz) while the bandwidths which can be suitably irradiated are in the 10-100 kHz range. The other two advantages, however, have provided the impetus toward the growth of FT-NQR.

(1) Comparison with High Resolution NMR (HR-NMR)

In HR-NMR the width of the spectrum Δ is much less than the carrier frequency f_o; $\Delta/fo \leqslant 10^{-3}$ can be expected even in worst cases. In NQR however, the ratio Δ/f_o is often of order unity.

This implies that the NQR spectrum must be obtained one frequency interval at a time and cannot usually be displayed in one operation as in the case in HR-NMR.

2. Processing Techniques

Once FID or echo signals have been obtained, the proper FT treatment for each will yield the desired lineshape spectrum.[26,27] In this section the procedures the authors found most satisfactory are discussed.

The problem of phase correction for NQR spectra presents a particular problem not found in fixed-frequency spectrometers. The fact that the NQR spectrometer operates at variable frequencies means that instrumental phase shifts will be present for NQR signals which are not corrected for before final data collection. These phase shifts can be considerable and are of course also present in echoes, where the receiver dead time problem present for FID signals does not occur. In Table II the mathematical results

---

[26] R. Lenk and E. A. C. Lucken, Pure Applied Chem. 40, 199 (1974).

[27] A. Colligiani and R. Ambrosetti, Gazz. Chim. Italiana 106, 439 (1976).

for Lorentzian lineshapes are collected as guides to the solution of this problem.

The results in the Table show that the presence of phase shifts produces an admixture of absorption and dispersion modes in the case of FID signals, and a possible loss of intensity in echo signals. This problem can be avoided while at the same time the true Lorentzian line shape is preserved, if the modulus squared transform is computed for FID signals, and the modulus transform is computed for echoes. Thus the proper line shapes are obtained in each case regardless of the degree and source of phase shift without need for a separate "phase correction" subroutine.

In Figs. 14-21 the results of computer-simulated spectra are shown. An echo and a FID signal have been simulated for both Lorentzian and Gaussian lineshapes. Cosine, sine, the square of the modulus, and modulus transforms are computed and displayed. Figs. 14-17 are for no phase shift, while Figs. 18-21 have a phase shift of 30° in the time domain signals. Note that in all cases the conclusions discussed for proper data processing are borne out, mainly that the modulus squared transform should be used for FID signals, and the modulus transform should be used for echo signals.

Figs. 22-24 show experimental spectra that demonstrate the foregoing arguments. Figs. 22(a) and 23(a) are the Nitrogen-14 NQR FID signals at 77°K from hexamethylenetetramine (HMT) and urea, respectively. The cosine and sine transforms of HMT, Figs. 22(b) and (c), clearly show the admixture of adsorption and dispersion expected when phase shifts exist in the time-domain data. This effect is much less evident in the cosine and sine transforms of urea, Figs. 23(b) and (c), which occurred with only a small phase shift. Finally, the proper lineshapes are shown in Figs. 22(d) and 23(d), the modulus squared

TABLE II

Lorentzian FID and echo complex signals and their Fourier transforms

FID

Time domain: $f(t) = e^{-\alpha t} e^{i\omega_o t} e^{-i\phi} \quad t \geq 0$

C, Cosine transform $= \dfrac{1}{\alpha^2+(\omega-\omega_o)^2}\left\{\alpha\cos\phi - (\omega-\omega_o)\sin\phi\right\}$

S, Sine transform $= \dfrac{1}{\alpha^2+(\omega-\omega_o)^2}\left\{\alpha\sin\phi + (\omega-\omega_o)\cos\phi\right\}$

C^2+S^2, Modulus squared **transform** $= \dfrac{1}{\alpha^2+(\omega-\omega_o)^2}$

$[C^2+S^2]^{\frac{1}{2}}$, Modulus transform $= \left[\dfrac{1}{\alpha^2+(\omega-\omega_o)^2}\right]^{\frac{1}{2}}$

ECHO

Time domain: $f(t) = \begin{cases} e^{\alpha t} e^{-i\omega_o t} e^{-i\phi} & t < 0 \\ e^{-\alpha t} e^{i\omega_o t} e^{-i\phi} & t \geq 0 \end{cases}$

C, Cosine transform $= \dfrac{1}{\alpha^2+(\omega-\omega_o)^2} 2\alpha\cos\phi$

S, Sine transform $= \dfrac{1}{\alpha^2+(\omega-\omega_o)^2} 2\alpha\sin\phi$

C^2+S^2, Modulus squared **transform** $= \left[\dfrac{2\alpha}{\alpha^2+(\omega-\omega_o)^2}\right]^2$

$[C^2+S^2]^{\frac{1}{2}}$, **Modulus transform** $= \left[\dfrac{2\alpha}{\alpha^2+(\omega-\omega_o)^2}\right]$

transforms of the time-domain signals. Note the fine structure on the HMT line, first reported by Colligiani and Ambrosetti.[28] The modulus transforms, Figs. 22(e) and 23(e), are shown for comparison and they are visibly broader than the true lineshapes.

An example of an echo signal is shown in Fig. 24(a), a doublet of ν_- lines from the monoclinic phase of TNT at 77°K. Figs. 24(b) and (c) are, respectively, the cosine and sine transforms of this signal. Note that, as expected, both of these transforms yield valid lineshapes with fractional amplitudes, and that the modulus transform, Fig. 24(e), yields the correct lineshape.

IV. APPLICATIONS

The current intense interest in the chemistry, physics, and crystallography of solids is responsible for the renewed activity in NQR. In 1964 Grechishkin and Soifer[29] suggested specific applied categories into which NQR could be divided. These have been updated and include:

a. Investigation of the nature of chemical bonds in solids. (The NQR frequency is directly dependent upon the type of hybridization and the degree of ionization of the chemical bond.)

b. Establishment of nonequivalence of the location of resonant atoms in crystal lattices and molecules.

c. Qualitative analyses (each chemical compound has a definite NQR spectrum).

d. Inspection of purity of chemical synthesis products (The NQR line

---

[28] A. Colligiani and R. Ambrosetti, J. Chem. Phys. 60, 1871 (1974).

[29] V. S. Grechishkin and G. B. Soifer, Pribory i Tekhnika Eksperimenta 1, 5, (1964) (Russian).

intensity is directly dependent on the amount of soluble impurities in a sample.)

e. Structural analysis of crystals. (NQR is a valuable compliment to x-ray methods.)

f. Detection of phase transitions in crystals and the investigation of their kinetics.

g. Measurement of average rotary vibration frequencies and average moments of inertia of molecules in crystals, from the temperature dependence of NQR lines.

h. Measurement of strain.

i. Determination of temperature.

Table III lists some of the capabilities of NQR. These examples have been chosen because they represent real, current-day problems which have been presented for possible solution using NQR.

Table III

Suggested Applications of FT-NQR*

Characterization of new compounds (drugs, chemicals, explosives, liquid crystals, etc.).

Degree of crystal order (in clays, solid solutions, etc.).

Locus of aluminum atoms in plagioclase minerals.

Shelf life of materials (drugs, chemicals, explosives, etc.).

Determination of in-situ strain (salt domes, hard rock, etc.).

Detection of contraband (drugs, explosives).

Identification of contaminants (i.e. nature of N, S and O in coal).

Measurement of temperature.

Radiation damage in solids.

Crystalline polymorphism studies (i.e. relationship of TNT crystalline forms to impact stability, etc.).

Measurement of organic complexes (i.e. V, Cu, Ni in crude oil).

Identification of host minerals in bore-holes (i.e. measurement of uranium grade and type).

Characterization of phase transitions (i.e. in rock-forming minerals such as feldspars, pyroxenes, phyllosilicates, etc.).

Interpretation of crystal order with respect to thermodynamic properties (in minerals).

Determination of non-stoichiometric behavior (i.e. minerals, alloys single crystals, etc.).

Identification of small solid samples (i.e. exsolution in alumino-silicates, dangerous materials, rare compounds, etc.).

*In some instances NQR techniques other than FT may prove to be more suitable, i.e., double resonance NQR, acoustic NQR, etc.

V. CONCLUSIONS

It is now possible to anwser the two questions posed in the introduction. NQR development has been hindered by:

(a) Lack of proper instrumentation

(b) Inefficient sample excitation techniques

(c) Primitive data handling and processing methods.

It can be shown that solutions have been found for each of these drawbacks:

(a) Sensitive, high resolution, automated, pulsed NQR spectrometers which utilize state-of-the-art electronic, radar, and computer techniques fulfill the instrumentation needs.

(b) The availability and usability of a variety of pulse sequences such as spin-lock spin-echo (SLSE) or strong off-resonance comb (SORC) provide superior sample excitation.

(c) Fourier Transform data processing, using modulus squared or modulus transforms, represents the state-of-the-art procedure for the special NQR conditions.

The need for FT-NQR is clearly demonstrated by the examples given in Table III. The growing interest in understanding the behavior of solids has provided an impetus for analytical techniques suitable for use with solid state systems. Particular emphasis has been directed at natural systems, such as minerals, and military and security applications. Furthermore, the possibility of measuring in-situ strain is of major interest to the rock mechanics community. A technology which can measure both single crystals and polycrystalline materials, which can respond to contaminants or homogeneous small samples, which can operate both in the laboratory or under semi-remote conditions while providing high resolution spectral data for solid samples has

all of the versatility to develop into an important analytical method.

The authors wish to thank Mr. R. Connors of Block Engineering, Cambridge, MA for his assistance in running the NQR spectra. They would also like to recognize Mr. N. Henderson, Office of Nuclear Waste Isolation, Battelle-Columbus, Columbus, OH and Dr. C. Boghosian, U. S. Army Research Office, Research Triangle Park, N.C. for their continued support. Technical editing was done by Dr. Ellory Schempp of Lawrence Berkeley Laboratory, Berkeley, California.

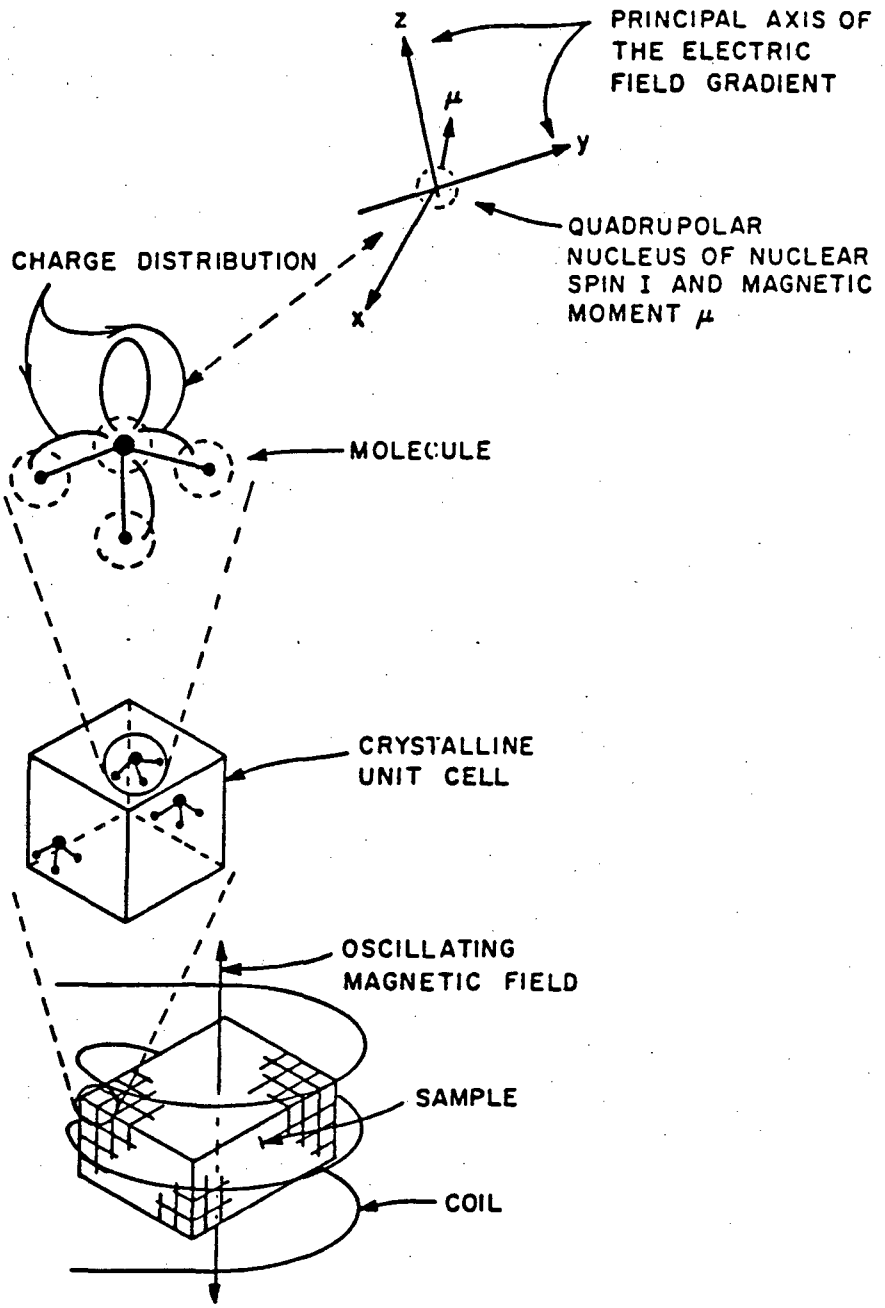

Figure I. Graphic Display for Nuclear Quadrupole Resonances.

XBL 793-8926A

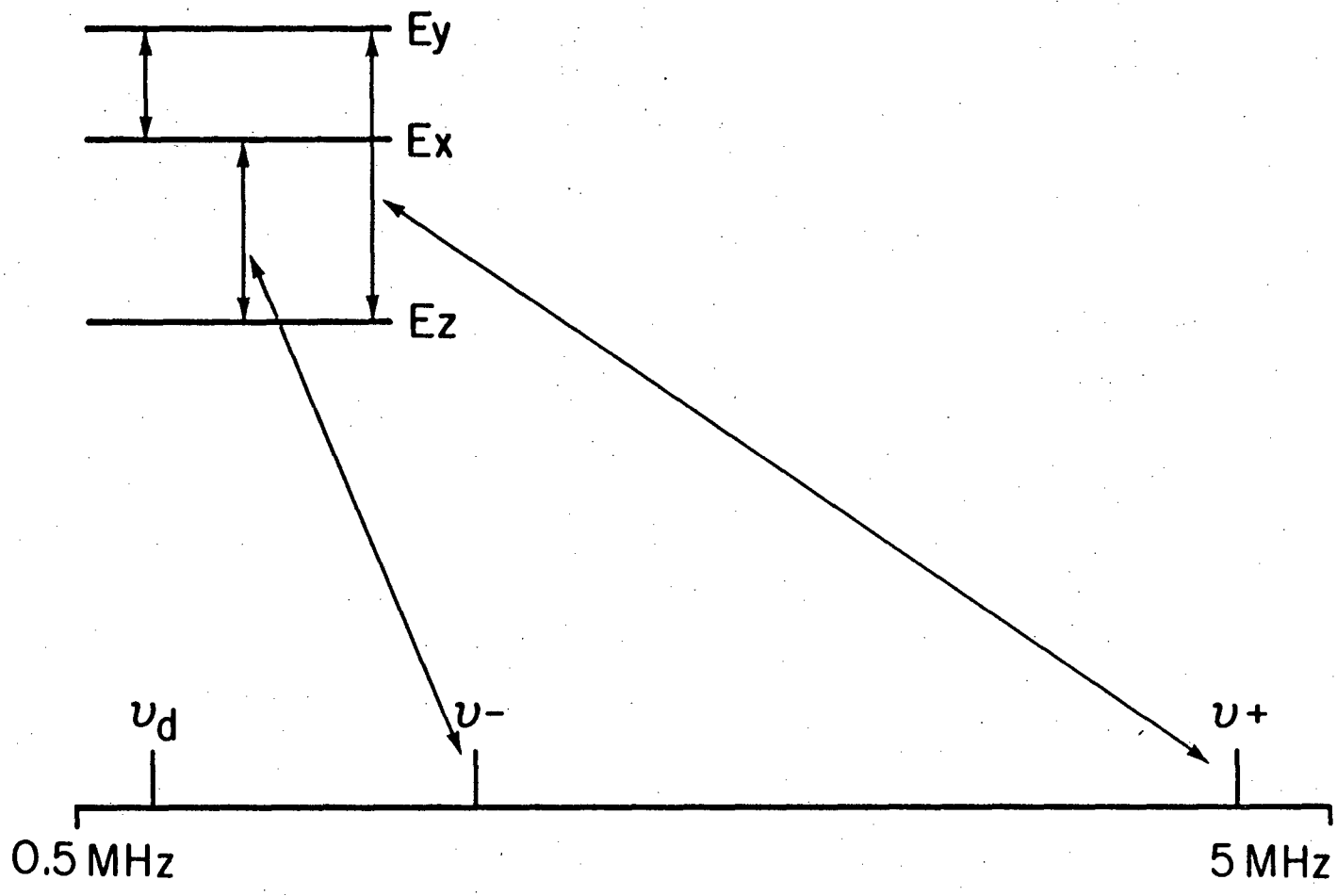

Figure 2. Energy Level Diagram and Approximate Frequency Range for Nitrogen-14 NQR.

XBL 808-2700A

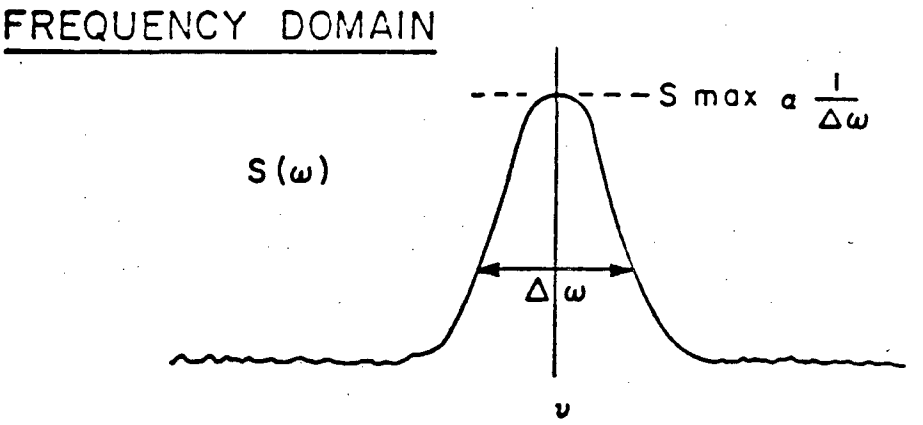

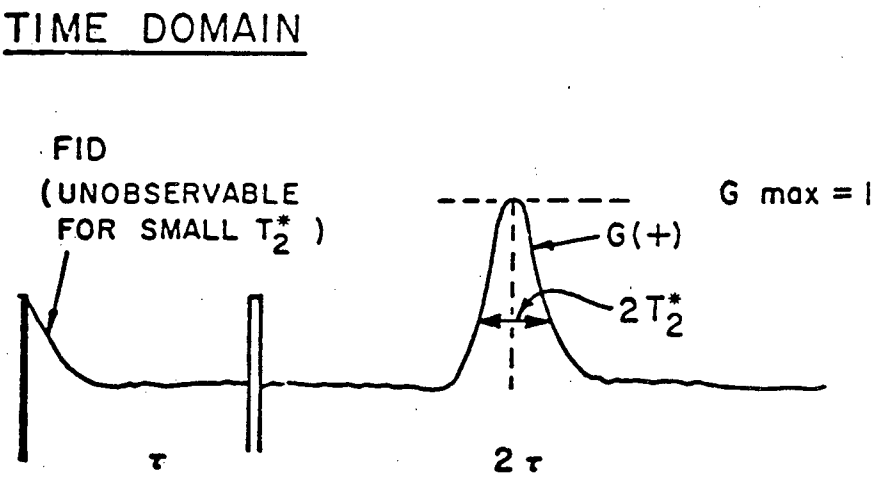

Figure 3. Line Shape Parameters for Spin Echo Sequence.

XBL 808-2701A

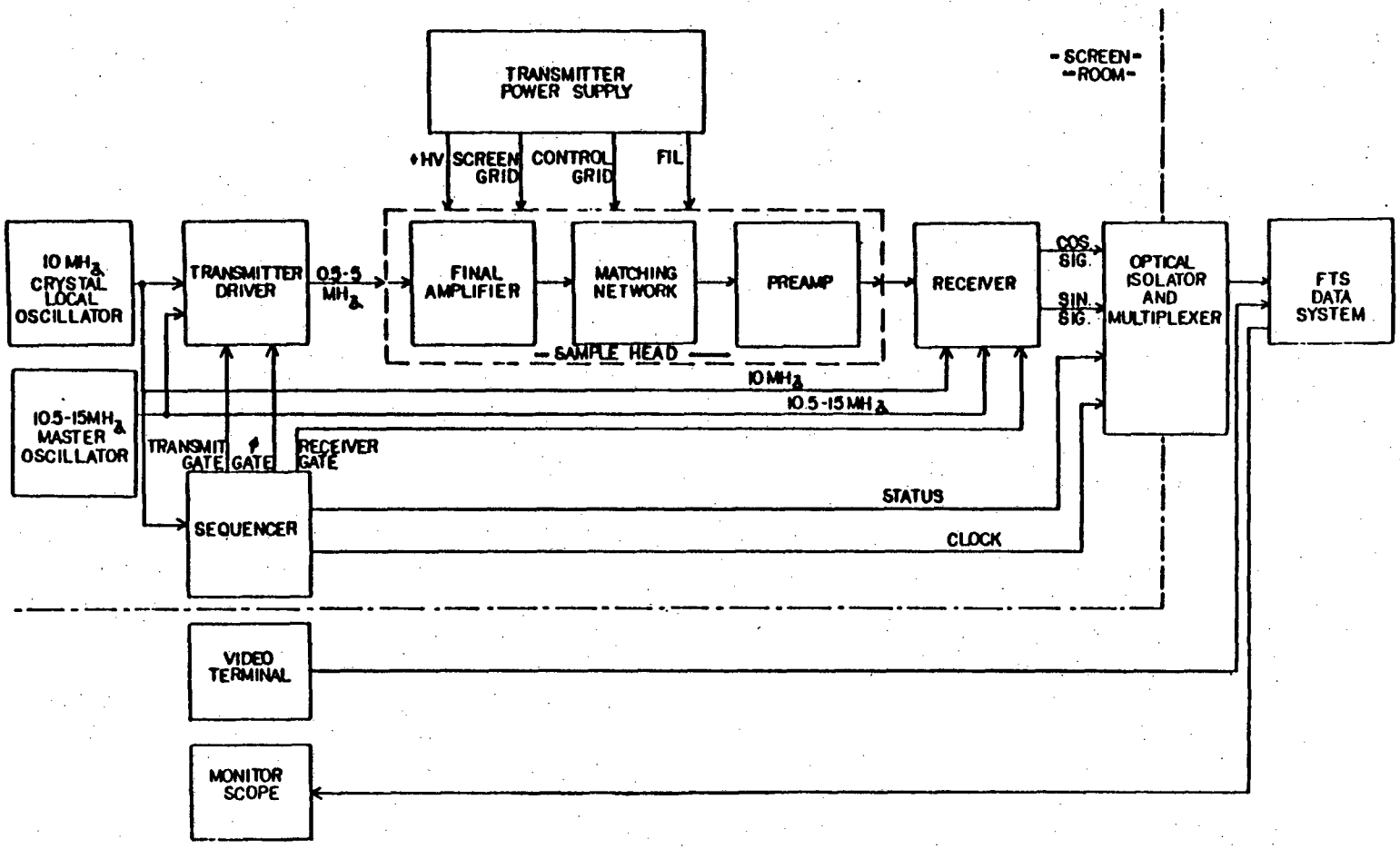

Figure 4. Block Diagram of the FT-NQR Spectrometer.

XBL 808-2702A

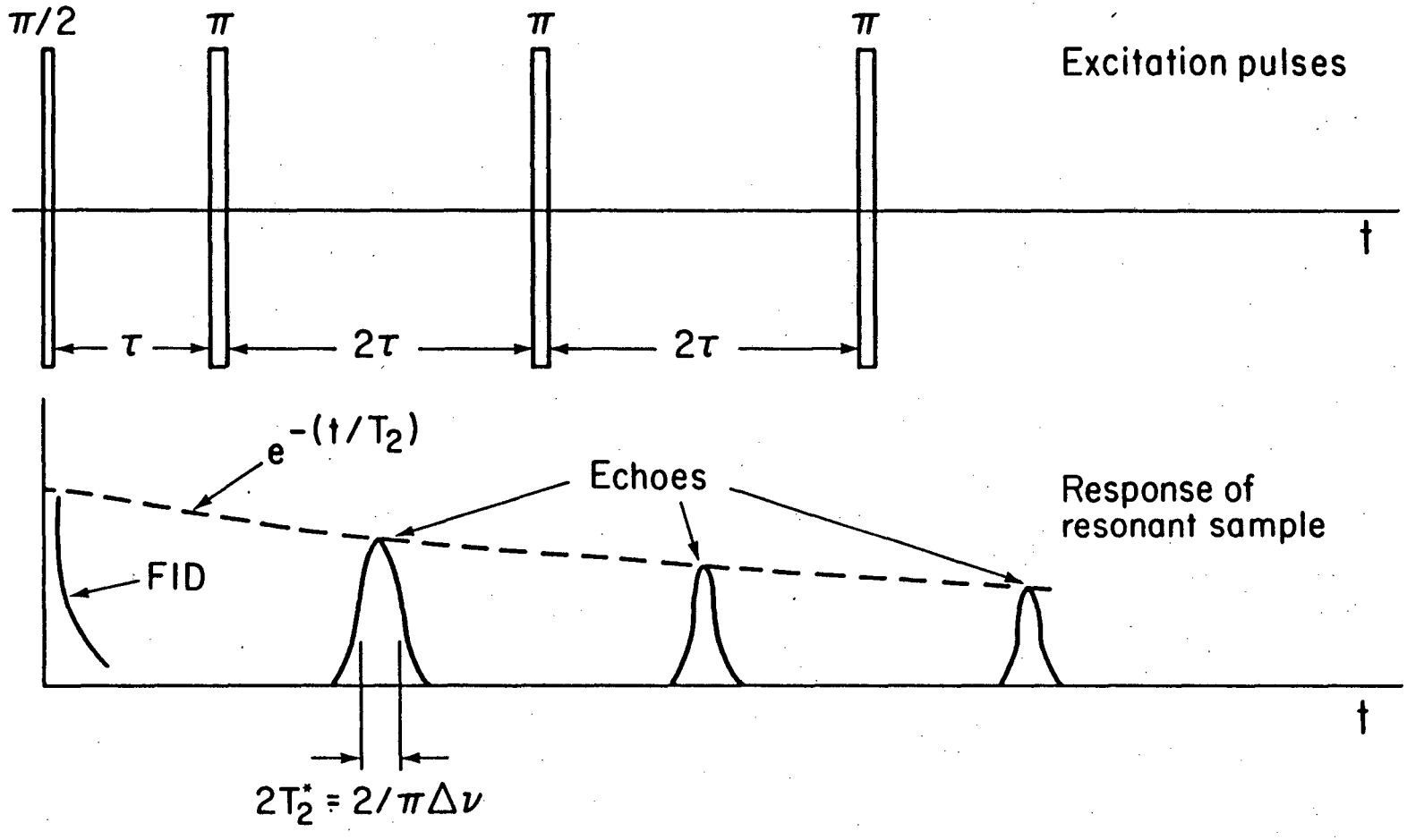

Figure 5. Parameters for the Carr-Purcell Sequence.

XBL 808 - 2703A

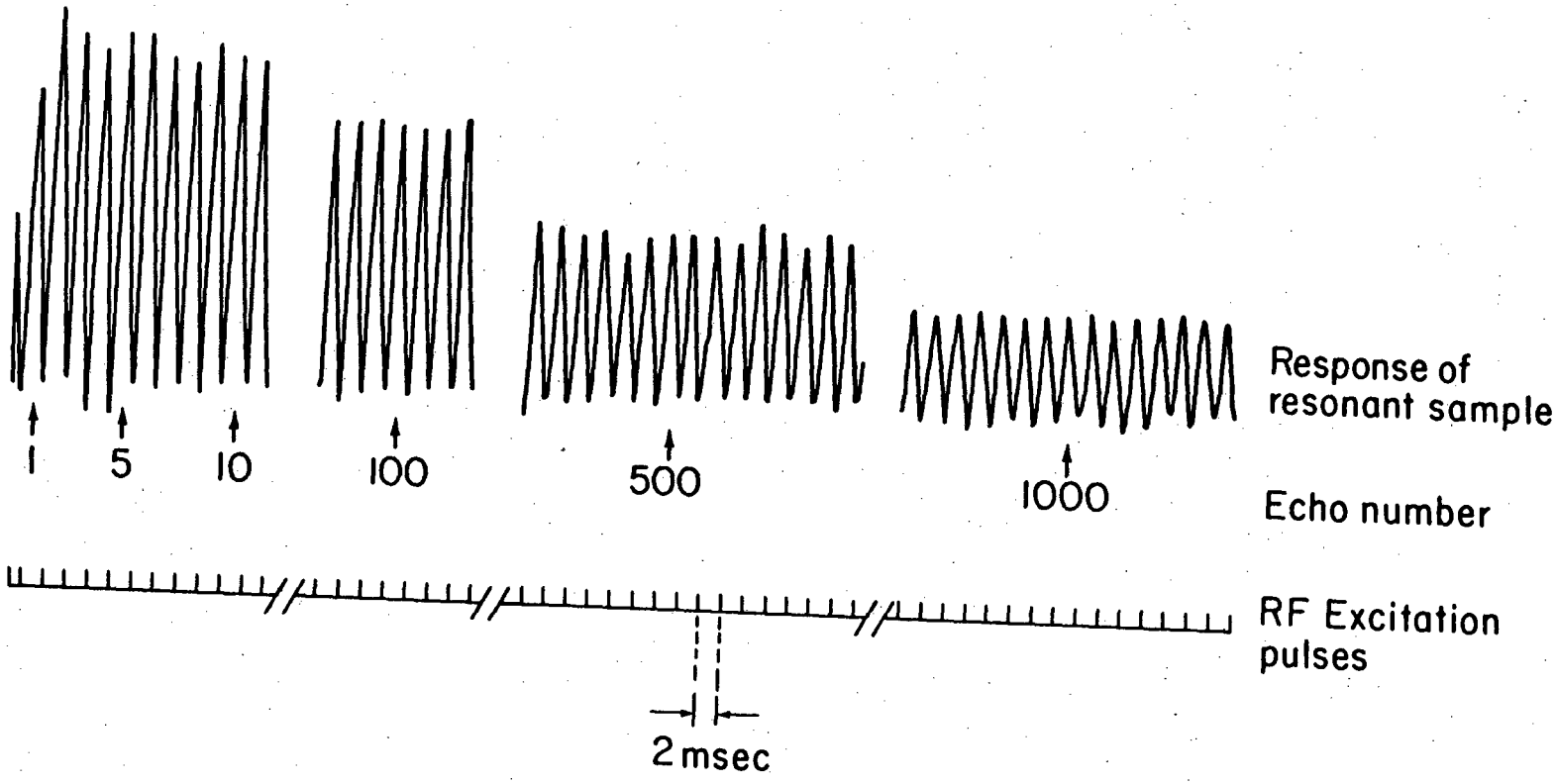

Figure 6. $NaNO_2$, 77 °K ν_- Line, On Resonance SLSE Sequence

XBL 808-2710A

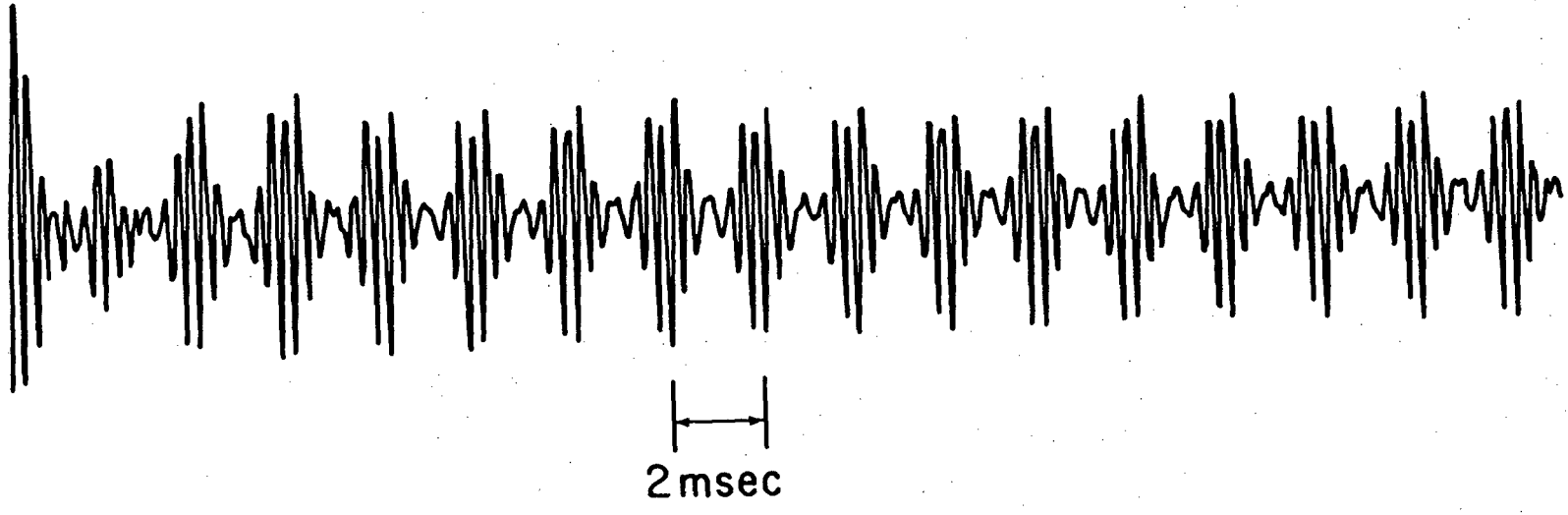

Figure 7. $NaNO_2$, 77 °K ν_- Line, Off-Resonance SLSE Sequence

XBL 808-2711A

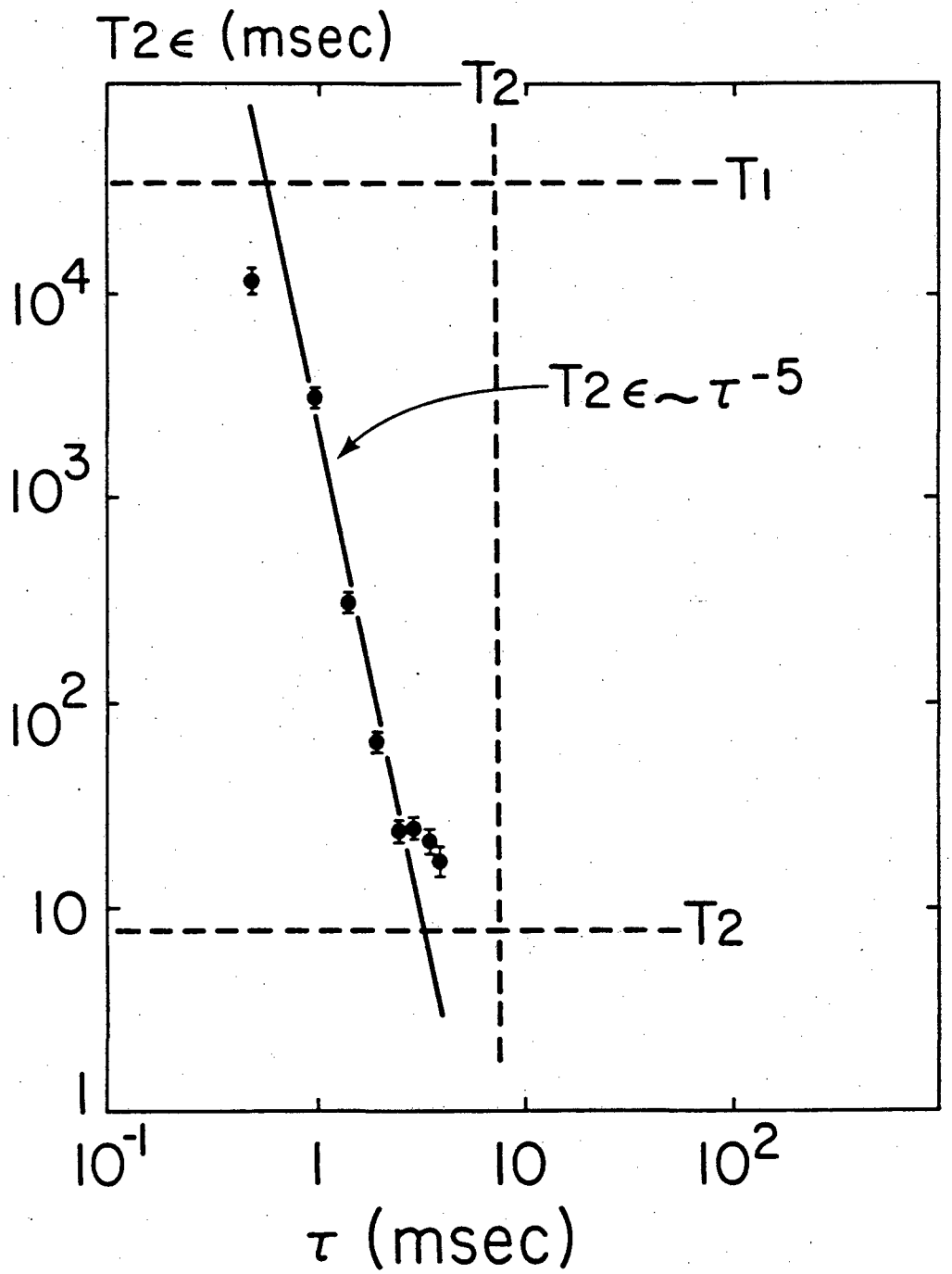

Figure 8. Echo Train Decay Constant, $T2\epsilon$ vs. SLSE Pulse Spacing τ for the ν_- Line of $NaNO_2$ at 77 °K

XBL 808 - 2704A

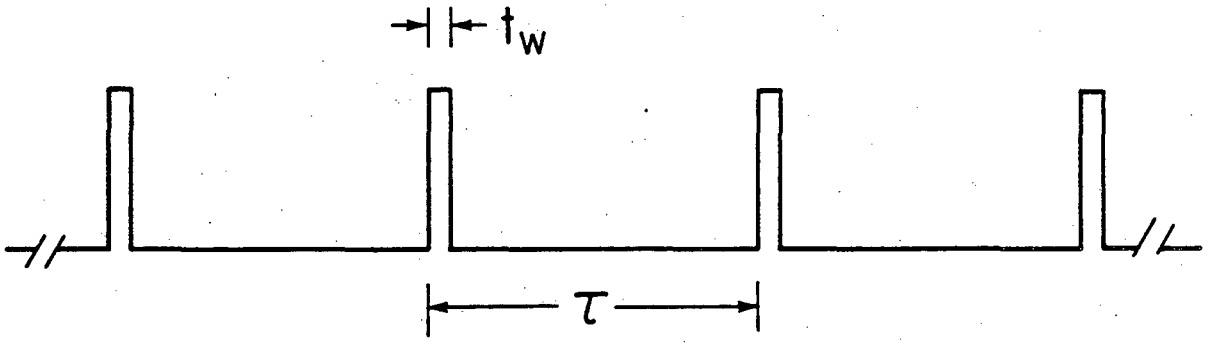

(a) Parameters

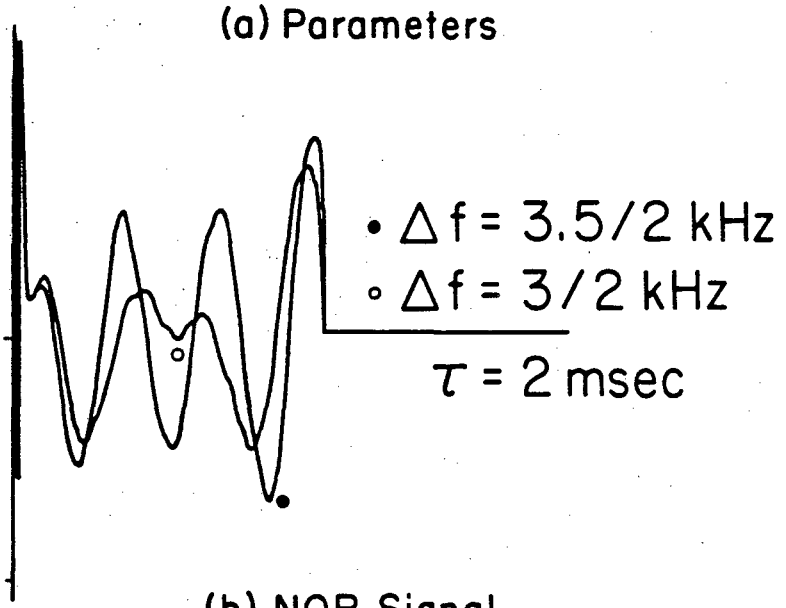

(b) NQR Signal

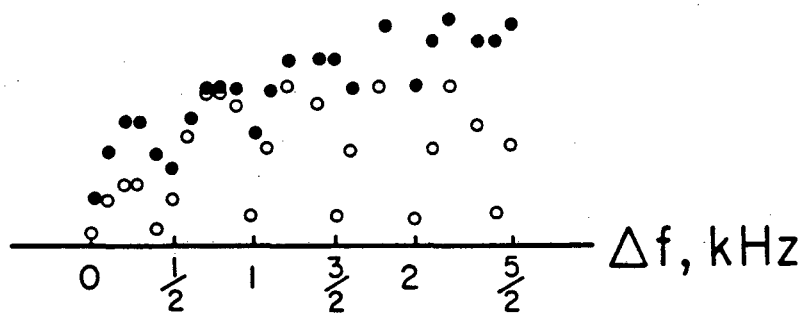

(c) NQR Signal vs. Resonance Offset

Figure 9. SORC Pulse Sequence

XBL 808 - 2705A

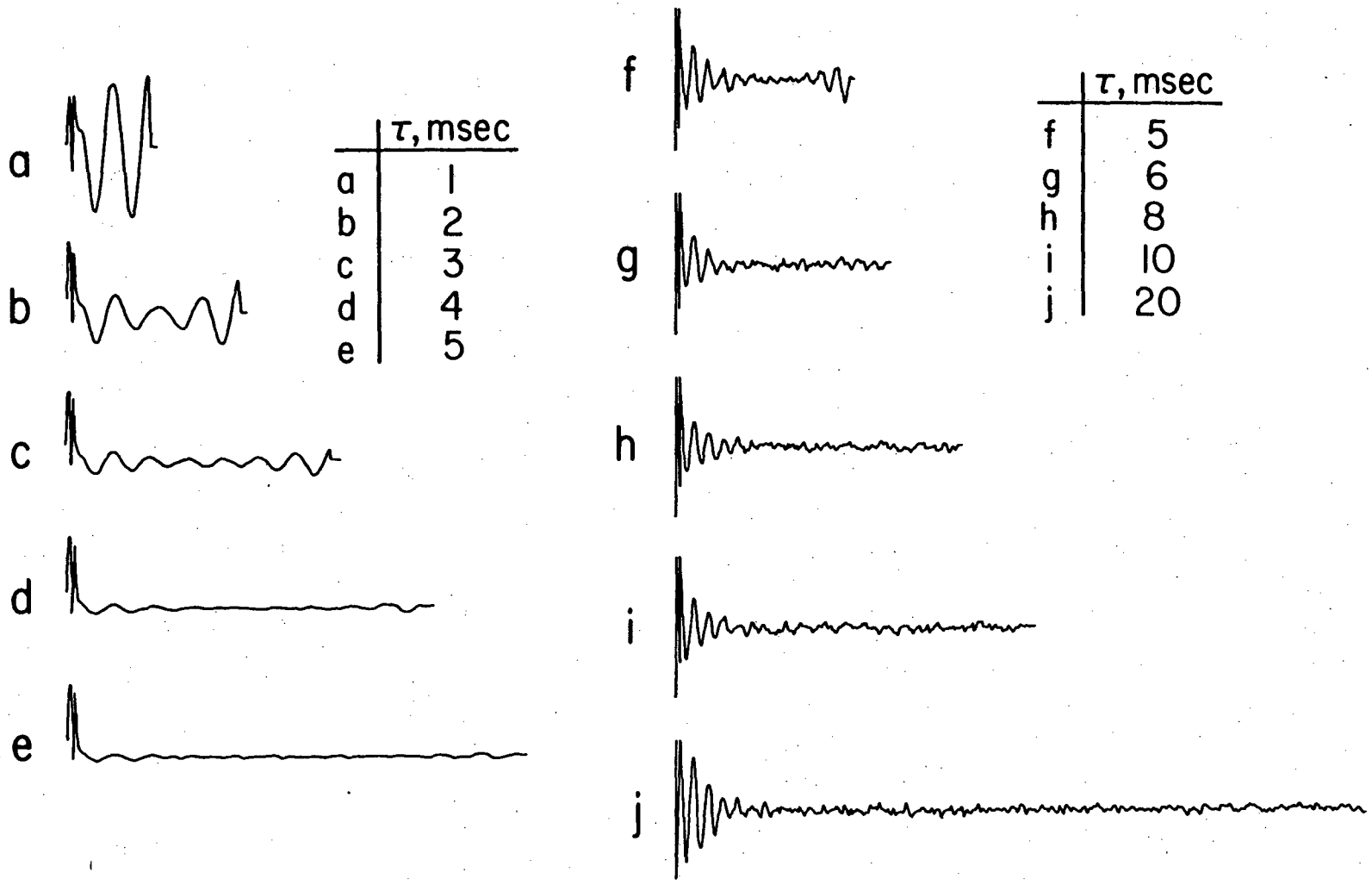

Figure 10. Steady State SORC Signal vs. τ

XBL 808-2706A

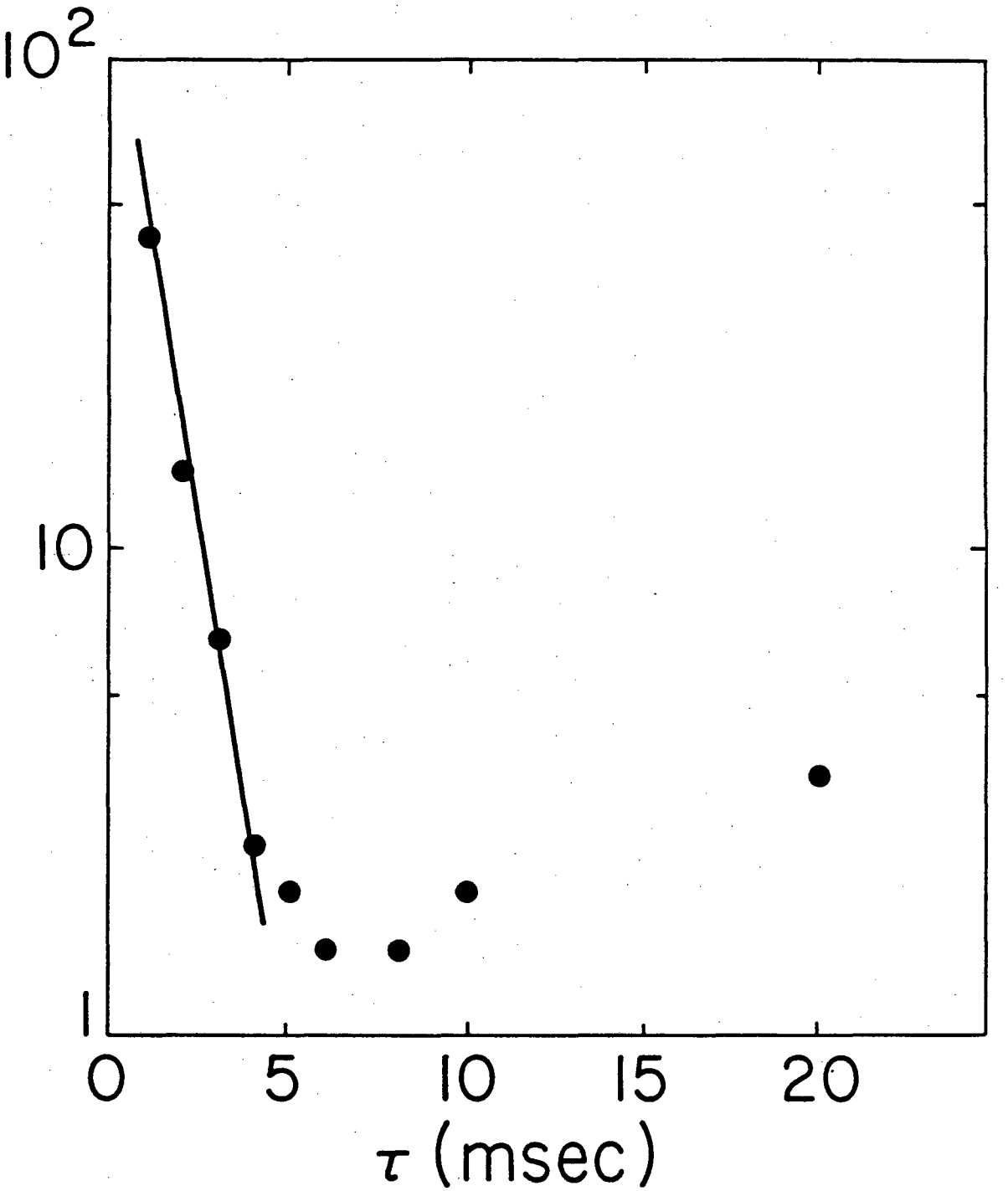

Figure 11 . Semilog Plot of SORC Signal vs. τ

XBL 808-2707A

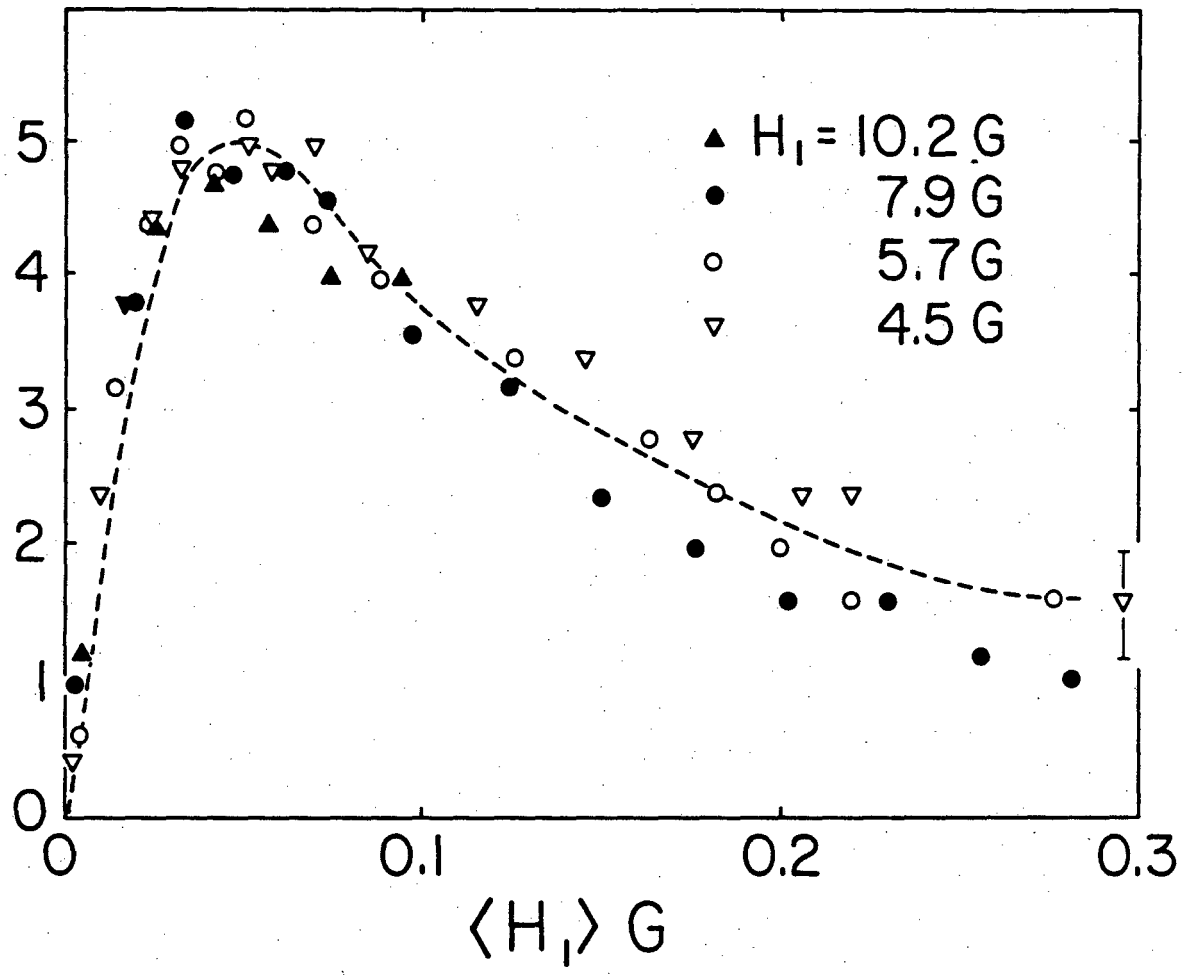

Figure 12. Size of SORC Signal vs. Average Value of H_1 (τ = 3 msec)

XBL 808-2708A

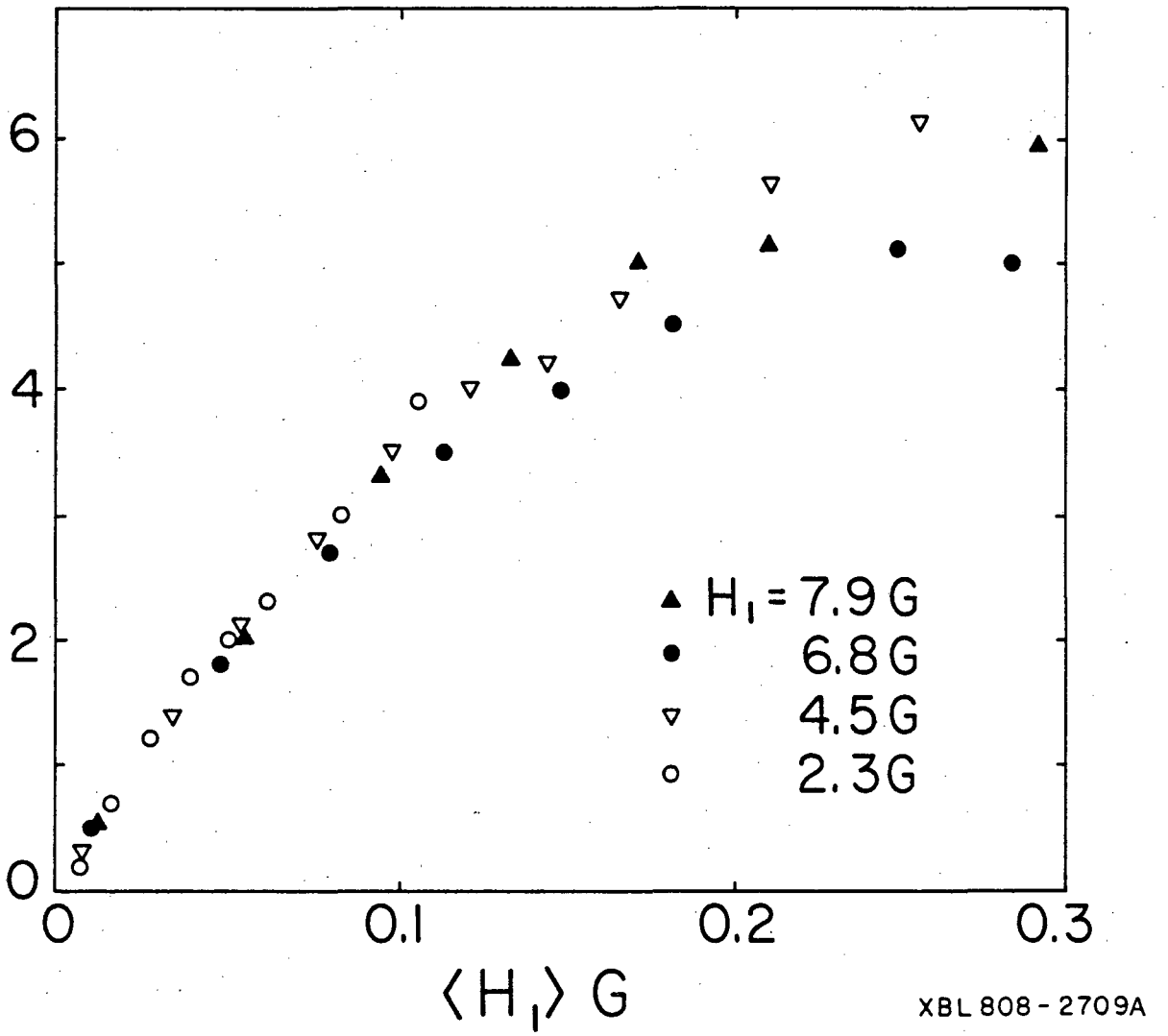

Figure 13. Size of SORC Signal vs. Average Value of H_1 (τ = 1 msec)

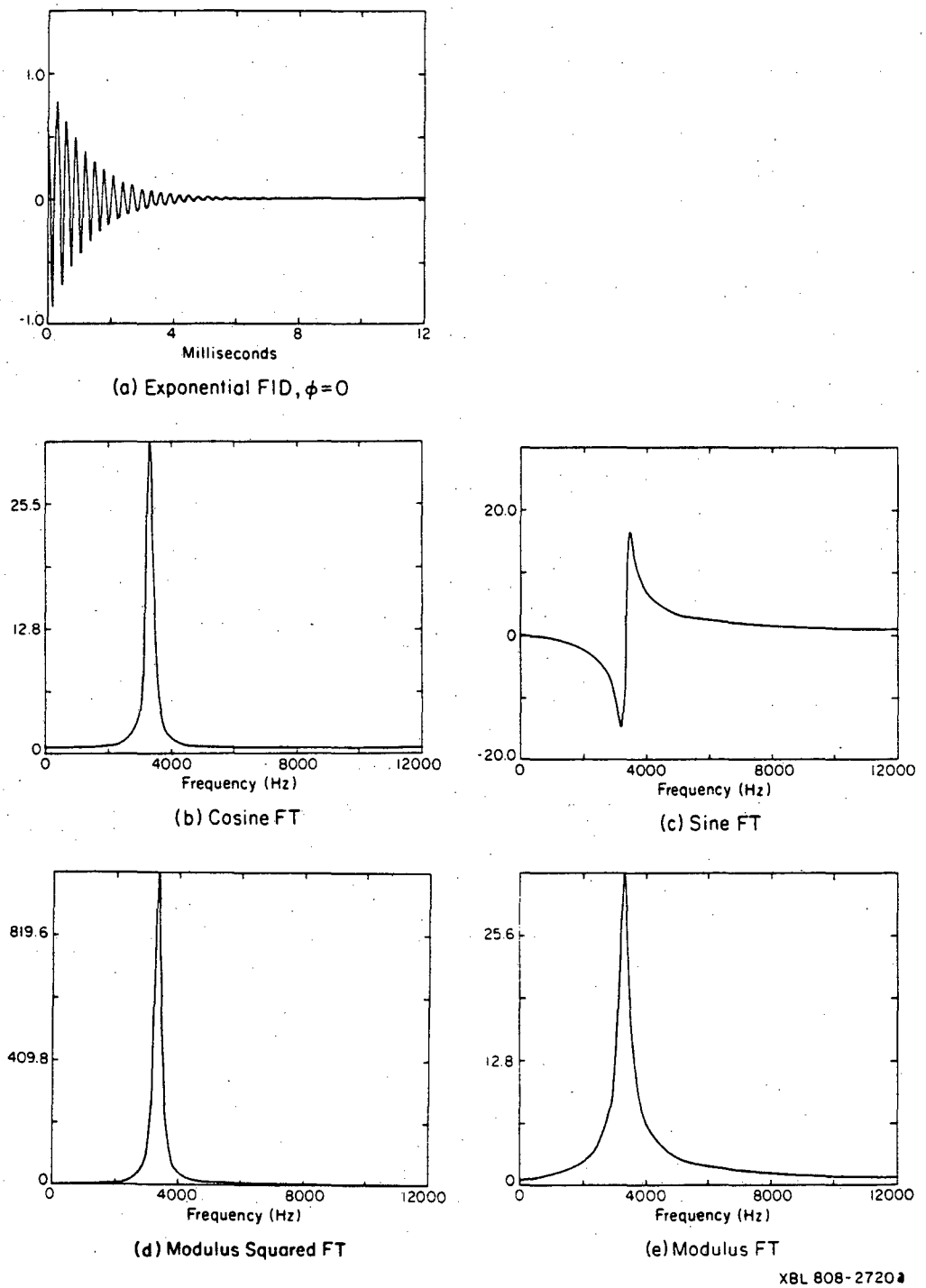

Figure 14. Simulated Exponential FID ($\phi=0$) and its Fourier Transforms

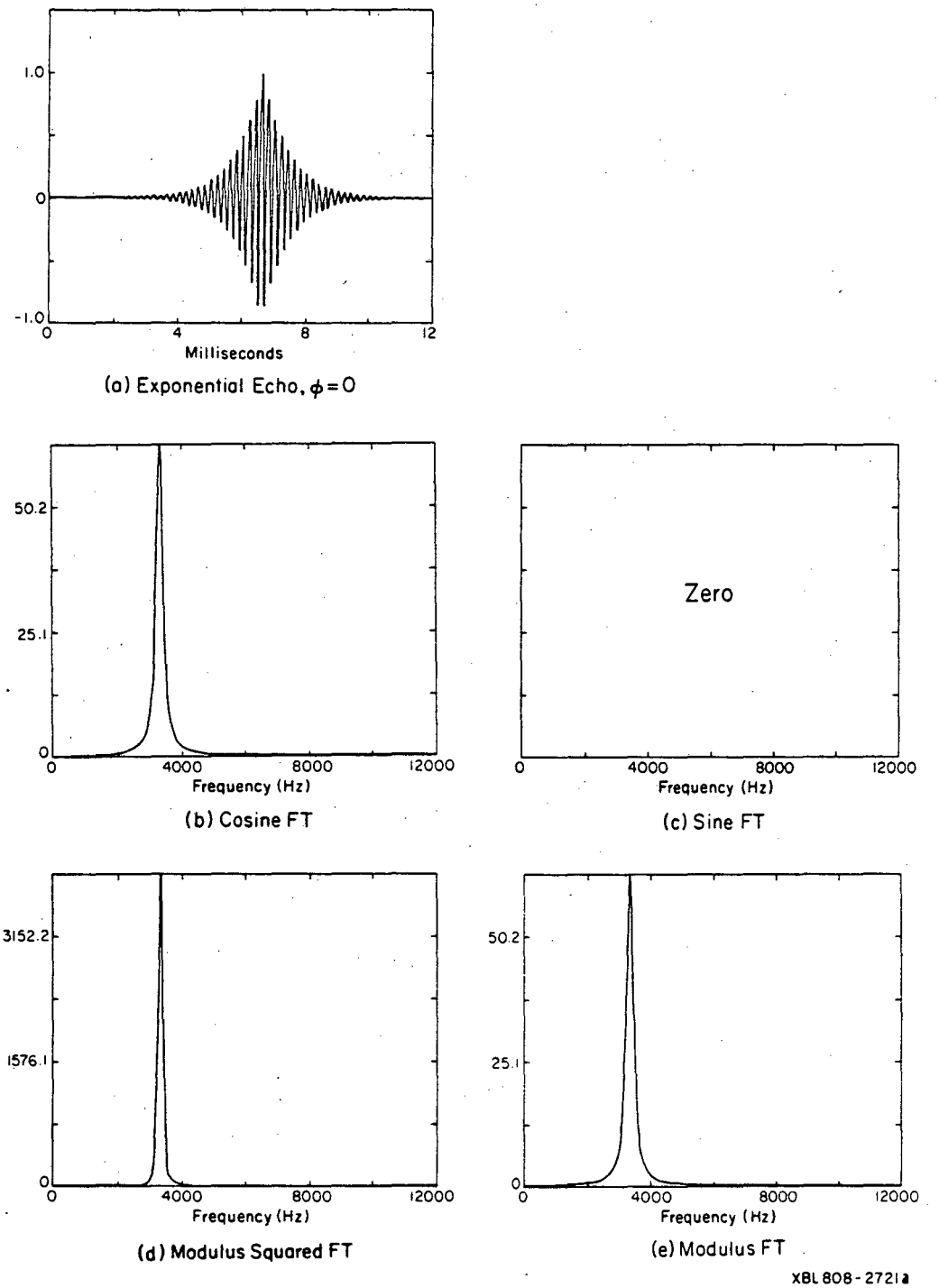

Figure 15. Simulated Exponential Echo ($\phi = 0$) and its Fourier Transforms

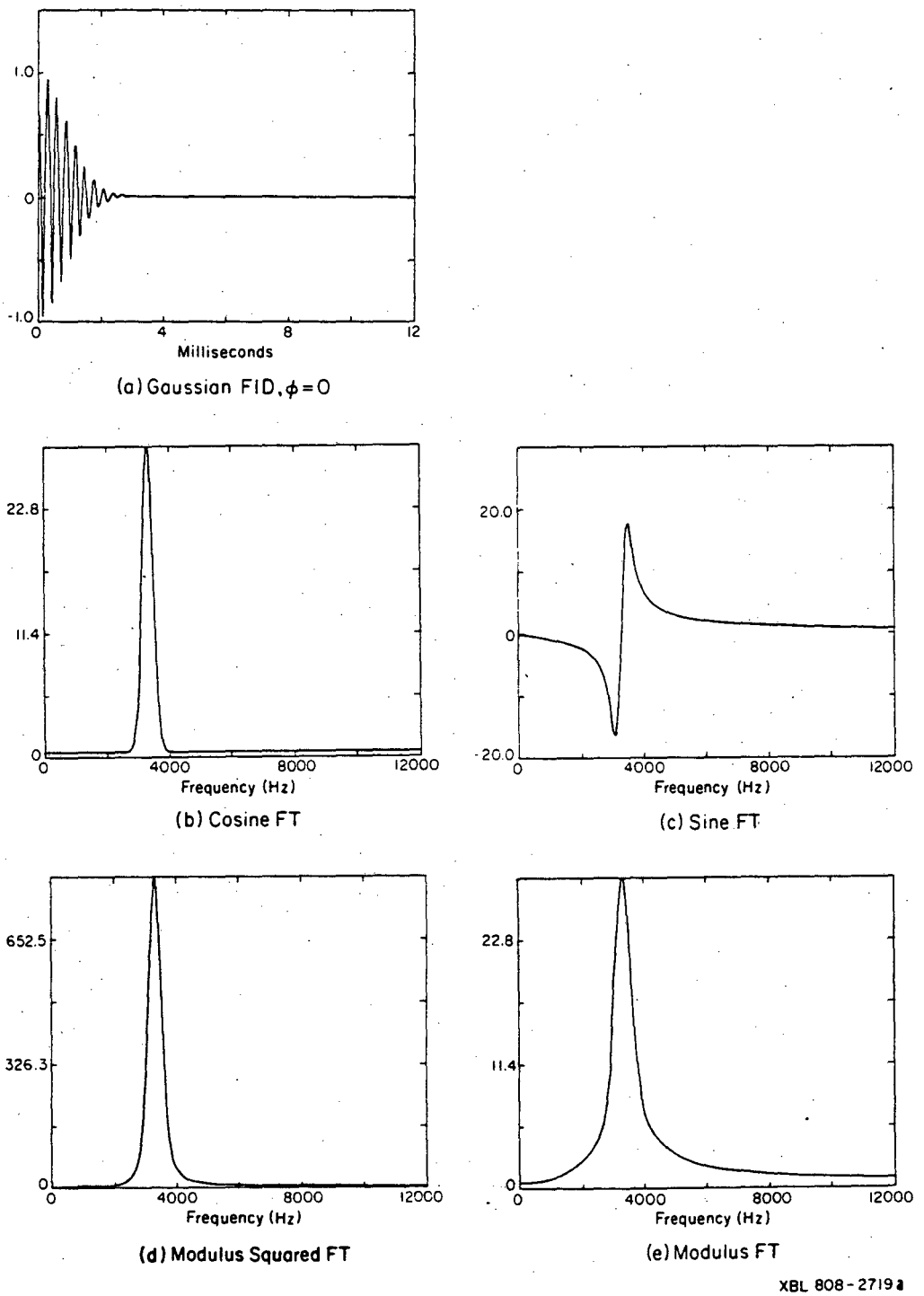

Figure 16. Simulated Gaussian FID ($\phi = 0$) and its Fourier Transforms

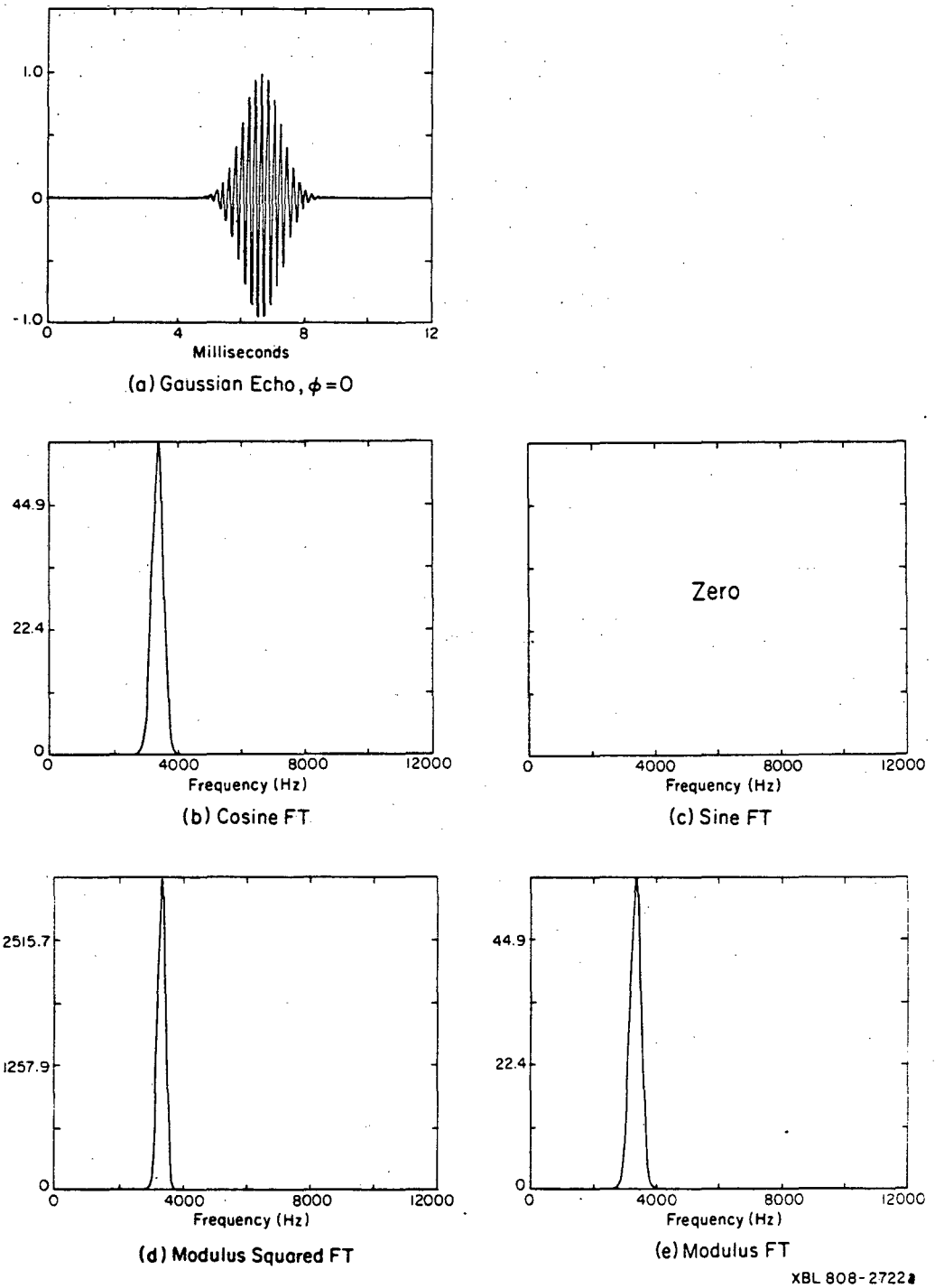

Figure 17. Simulated Gaussian Echo ($\phi = 0$) and its Fourier Transforms

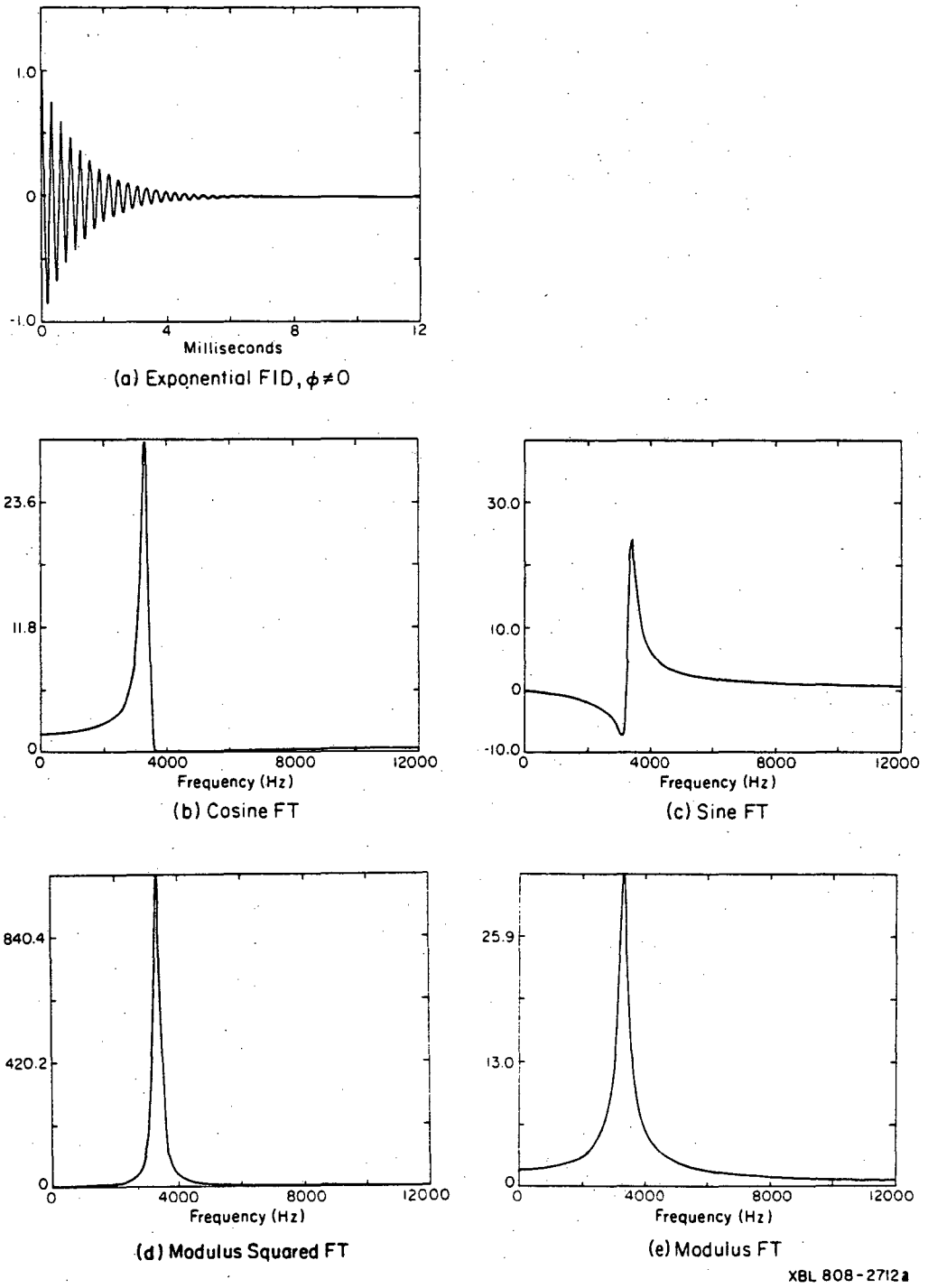

Figure 18. Simulated Exponential FID ($\phi \neq 0$) and its Fourier Transforms

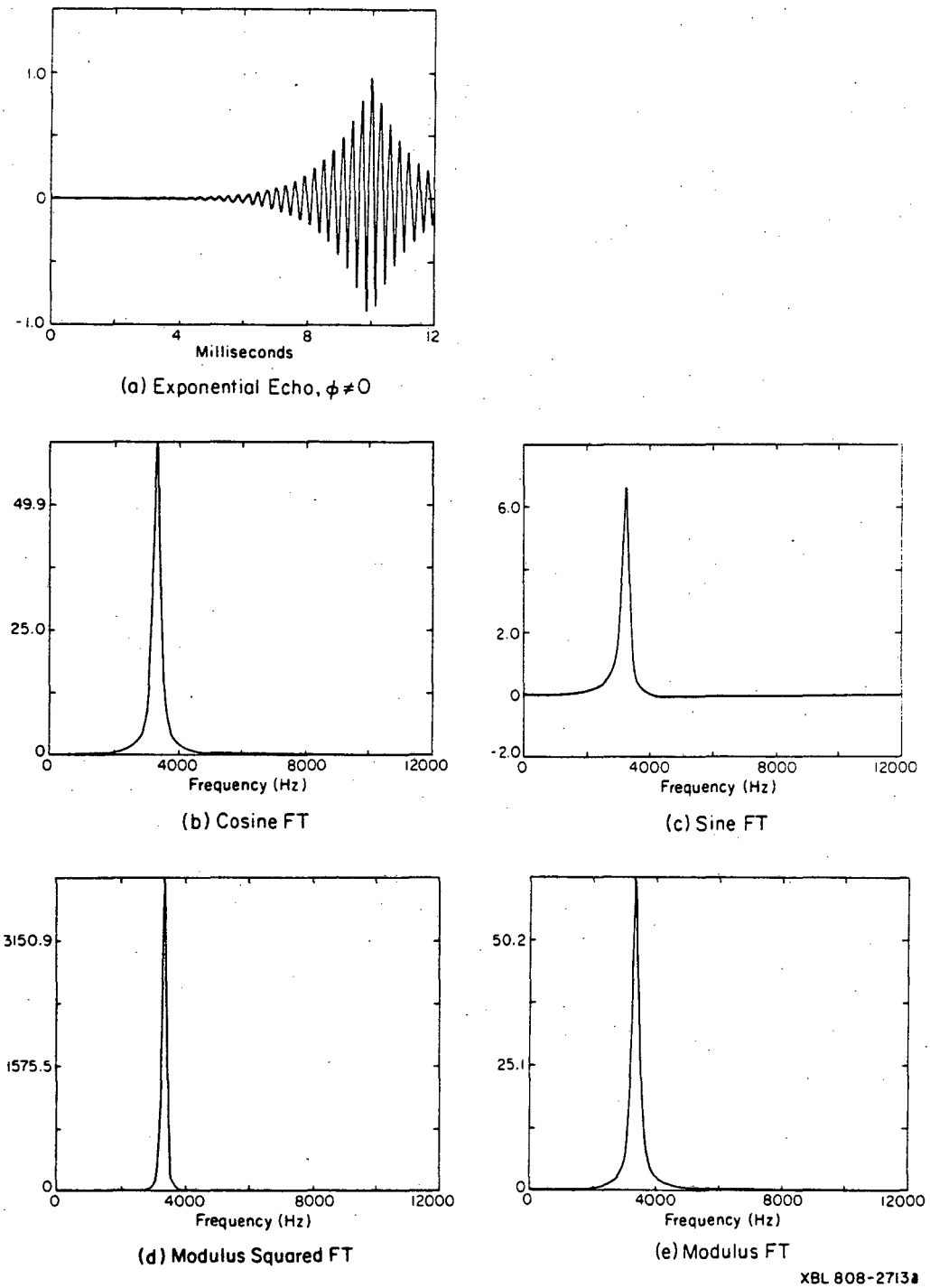

Figure 19. Simulated Exponential Echo ($\phi \neq 0$) and its Fourier Transforms

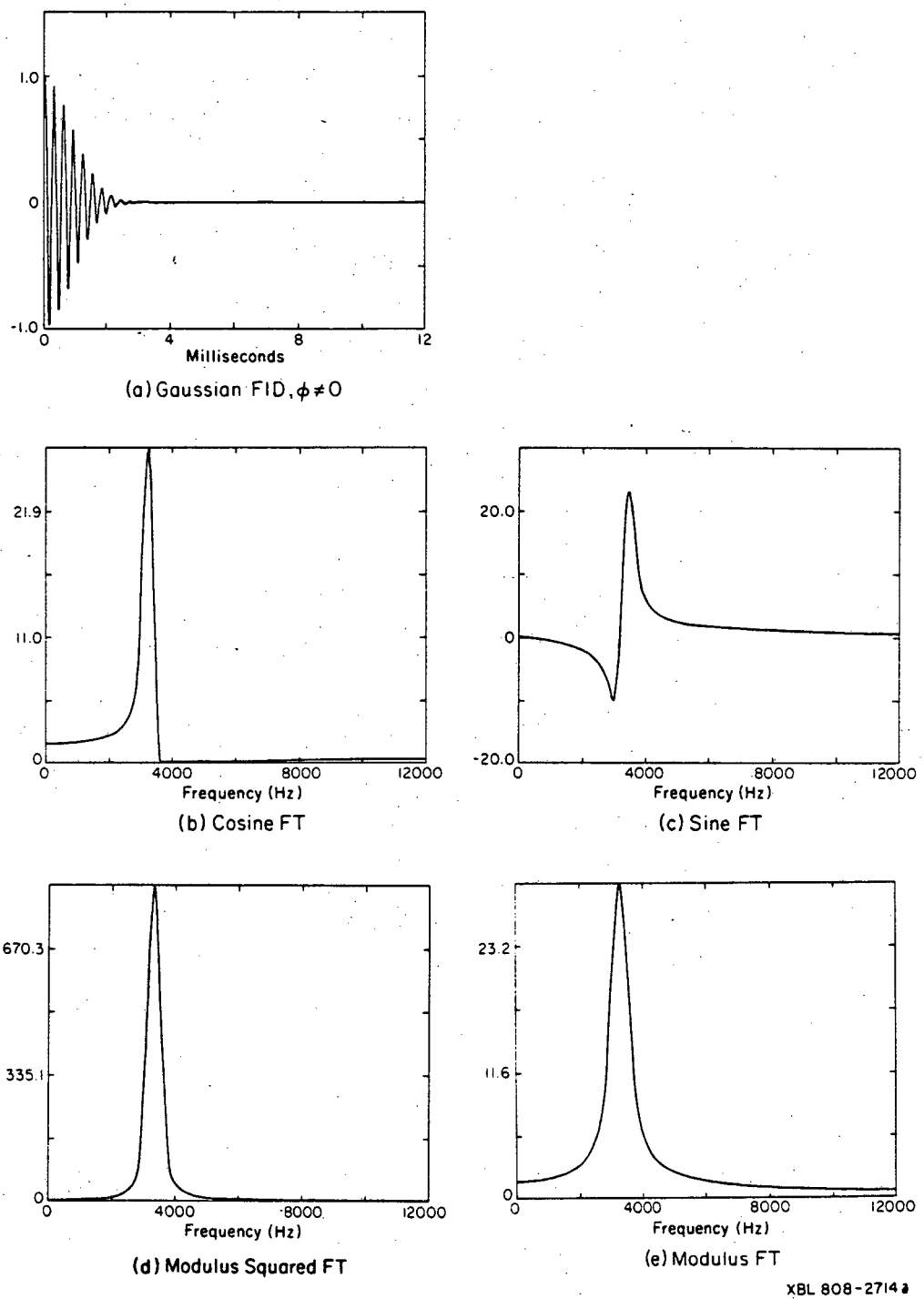

Figure 20. Simulated Gaussian FID ($\phi \neq 0$) and its Fourier Transforms

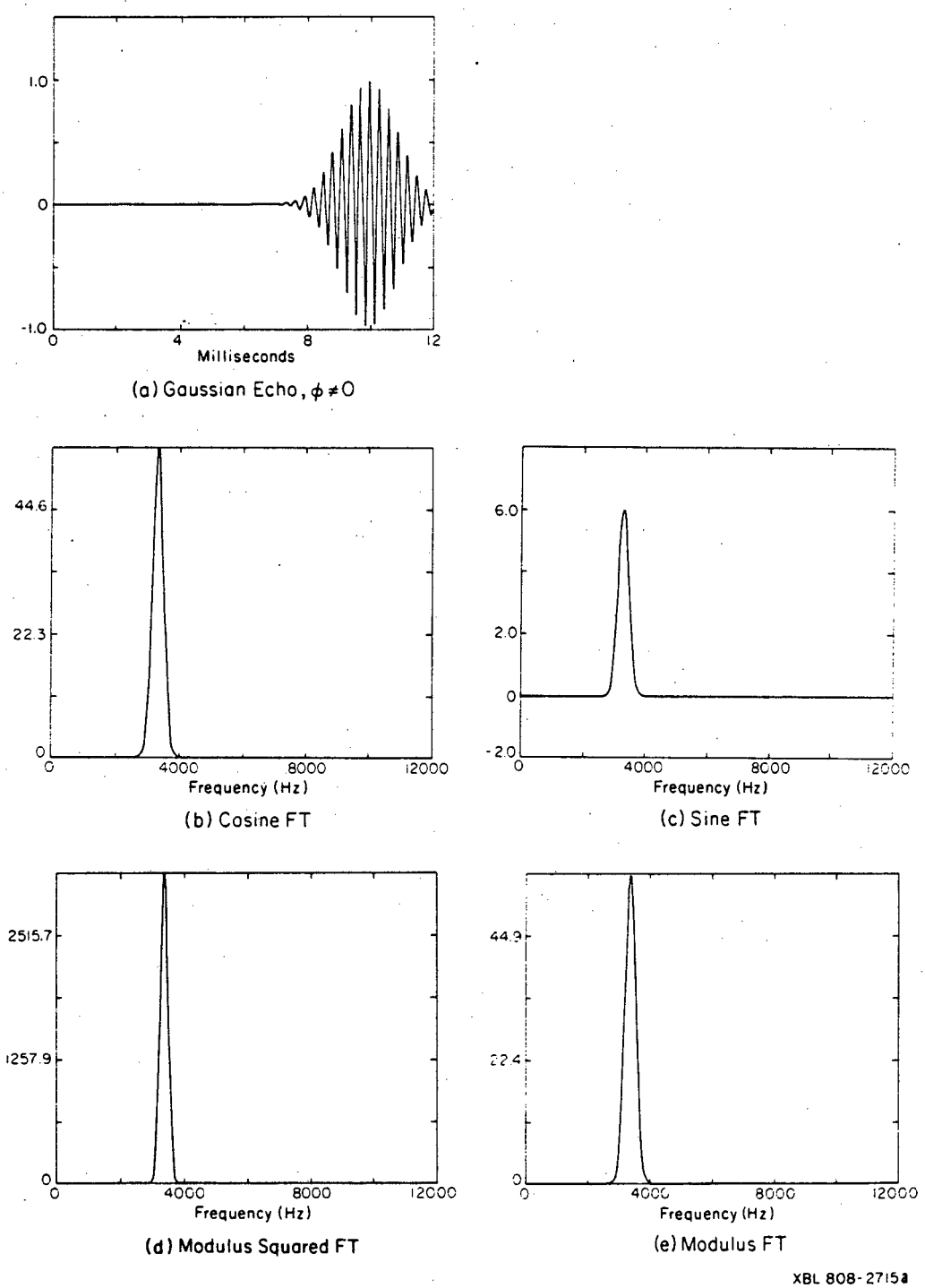

Figure 21. Simulated Gaussian Echo ($\phi \neq 0$) and its Fourier Transforms

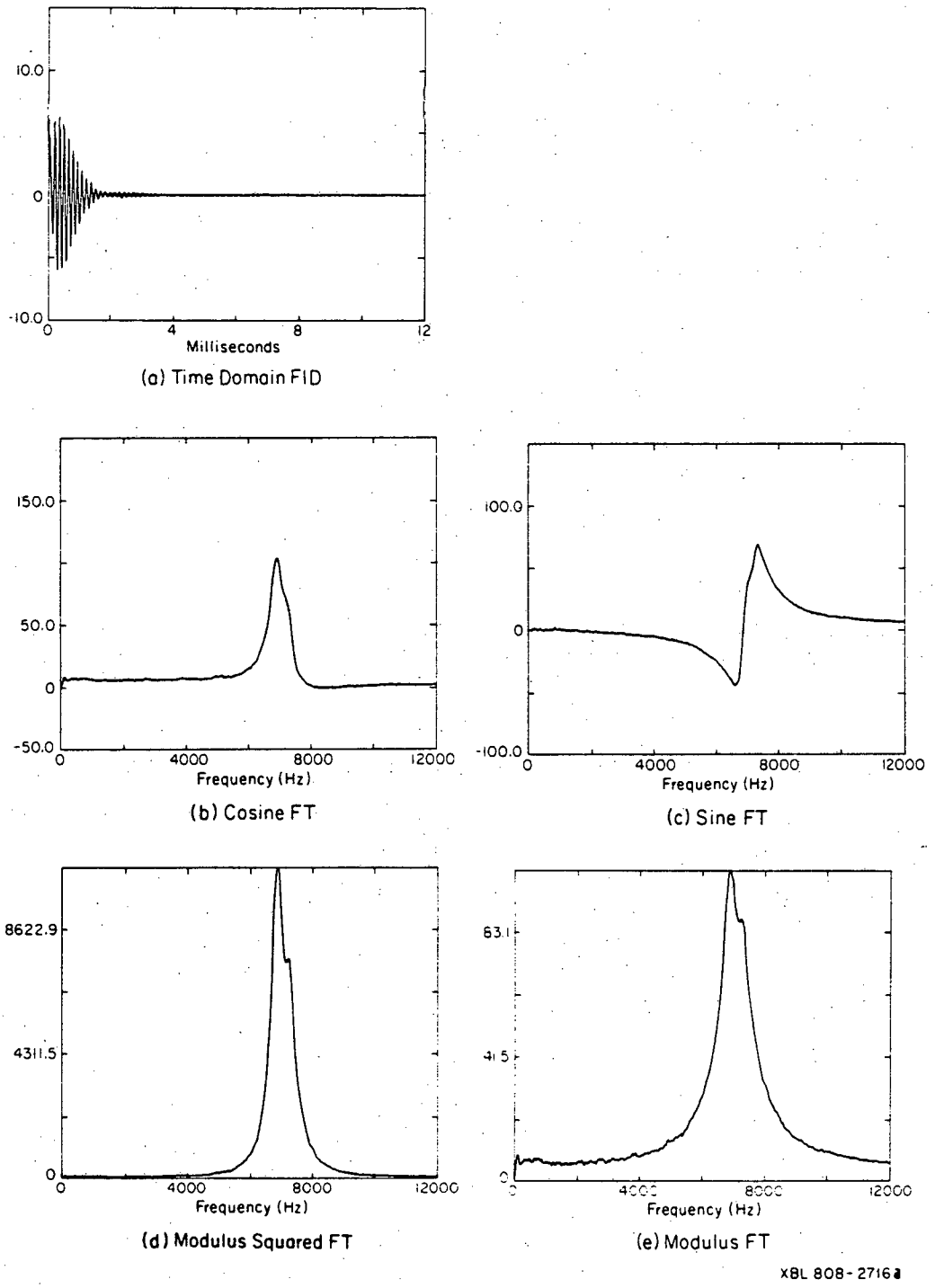

Figure 22. Hexamethylenetetramine, Room Temperature

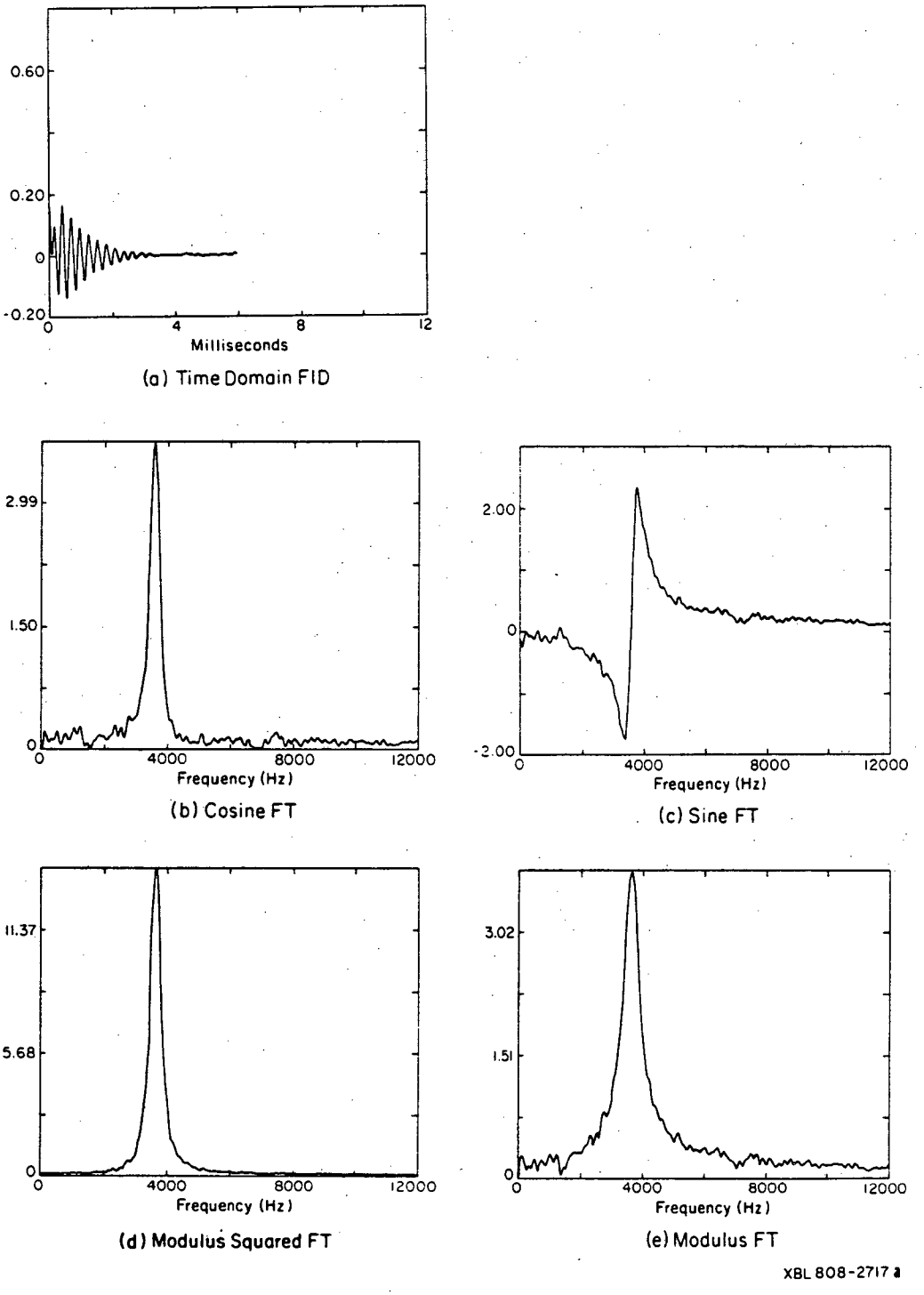

Figure 23. Urea, ν_+ Line at 77 °K

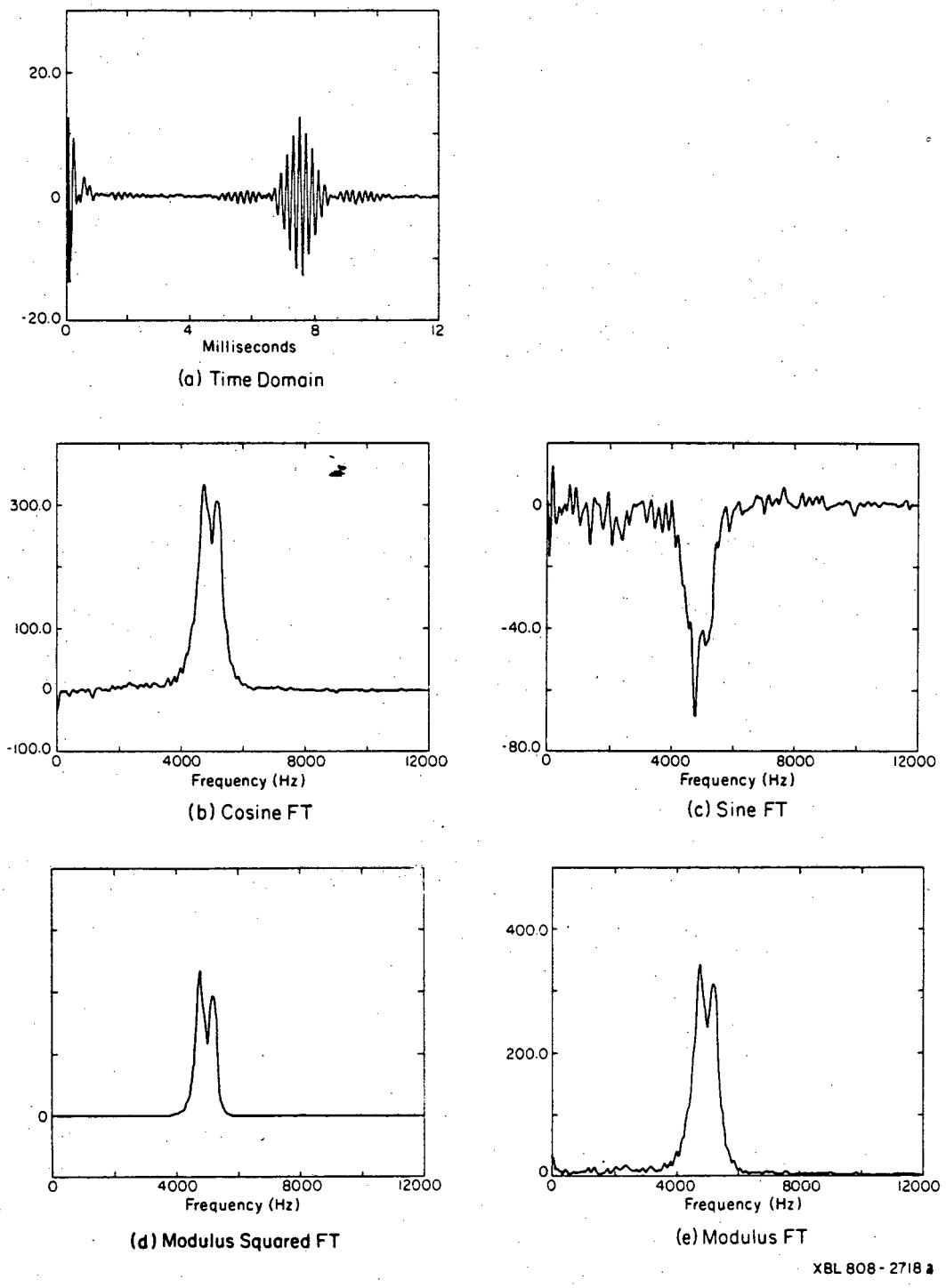

Figure 24. 727 kHz Doublet in Monoclinic TNT at 77°K

This report was done with support from the Department of Energy. Any conclusions or opinions expressed in this report represent solely those of the author(s) and not necessarily those of The Regents of the University of California, the Lawrence Berkeley Laboratory or the Department of Energy.

Reference to a company or product name does not imply approval or recommendation of the product by the University of California or the U.S. Department of Energy to the exclusion of others that may be suitable.

TECHNICAL INFORMATION DEPARTMENT
LAWRENCE BERKELEY LABORATORY
UNIVERSITY OF CALIFORNIA
BERKELEY, CALIFORNIA 94720